Morphology control of zinc oxide nanoparticles

Luís Filipe Marques Rodrigues

Thesis to obtain the Master of Science Degree in

Materials Engineering

Supervisor: Prof. Dr. Carlos Miguel Calisto Baleizão

Examination Committee

Chairperson: Prof. Dr. Alberto Eduardo Morão Cabral Ferro

Supervisor: Prof. Dr. Carlos Miguel Calisto Baleizão

Members of the Committee: Profª. Dra. Ana Clara Lopes Marques

November 2022

Acknowledgments

First, I would like to thank my supervisor, Prof. Dr. Carlos Baleizão, and Prof. Dr. José Paulo Farinha, for their guidance, suggestions and help in planning the work and discussing its results. It was a privilege for me to work with you and contribute to expand the knowledge in the nanotechnology field.

To all my laboratory partners and professors from OM^2 group, for all the help and guidance you gave me in the lab and for the good times we shared there.

To my dear mother, for all the love and support you have always given me and for encouraging me to put my best in everything I do.

To my close friends and family, for your friendship and for all the laughs and good times, which always gave me strength to finish this thesis.

To Associação Duarte Tarré, for all the support and for helping me to pursue my dreams.

Abstract

Zinc oxide is a metal oxide semiconductor that has aroused increasing interest in various fields of science due to its unique properties. The main objective of this work was to understand the growth mechanism of zinc oxide nanoparticles by the sol-gel method and how the synthesis parameters (pH, precursor concentration, solvent, reaction time and temperature) affect their final structure, namely their morphology and size.

The results showed that the formation of ZnO is favoured due to the higher concentration of OH^- and the nanoparticles size decreased with increasing pH value, in basic medium. The nanoparticles diameter also increased with decreasing precursor concentration and they were larger when the solvent used was water, compared to methanol. The reaction times analysed did not change the nanoparticles, and the temperature experiments were inconclusive, there was no clear morphological change with the temperature variation. In all experiments, the nanoparticles are spherical and most particle sizes are between 5 and 13 nm.

A second objective of this thesis was to develop mesoporous zinc oxide nanoparticles by the sol-gel method. Currently there are very few approaches to try to synthesize these particles and the existing ones still do not allow obtaining scalable and versatile syntheses, with well-defined morphologies, and controllable pore and particle sizes. To test the possibility of producing mesoporous zinc oxide nanoparticles, two sol-gel syntheses were performed, with one yielding mesoporous nanoparticles of about 107 nm. This method appears as a promising basis for a future development and optimization of mesoporous zinc oxide nanoparticles.

Key words: Zinc oxide; Nanoparticles; Mesoporous; Sol-gel synthesis.

Resumo

O óxido de zinco é um óxido metálico semicondutor que tem despertado um interesse crescente em diversas áreas da ciência, devido às suas propriedades únicas. O principal objetivo deste trabalho foi compreender o mecanismo de crescimento de nanopartículas de óxido de zinco pelo método sol-gel e como os parâmetros de síntese (pH, concentração do precursor, solvente, tempo de reação e temperatura) afetam a sua estrutura final, nomeadamente a morfologia e tamanho.

Os resultados mostraram que a formação de ZnO é favorecida por uma maior concentração de OH- e que o tamanho das nanopartículas diminui com o aumento do pH, em meio básico. O diâmetro das nanopartículas também aumentou com a diminuição da concentração do precursor e foi maior quando o solvente utilizado foi água, comparando com metanol. Os tempos de reação analisados não alteraram as nanopartículas, e as experiências de temperatura foram inconclusivas. Em todos as experiências, as nanopartículas são esféricas, com tamanhos compreendidos entre 5 e 13 nm.

Um segundo objetivo desta tese foi desenvolver nanopartículas mesoporosas de óxido de zinco por sol-gel. Atualmente existem poucas abordagens para sintetizar estas partículas e as existentes ainda não permitem a obtenção de sínteses escaláveis e versáteis, com morfologias bem definidas e tamanhos de partícula e poros controláveis. Para testar a possibilidade de produzir nanopartículas mesoporosas de óxido de zinco, foram realizadas duas sínteses sol-gel, originando uma delas nanopartículas mesoporosas com cerca de 107nm. Este método surge como uma base promissora para um futuro desenvolvimento de nanopartículas mesoporosas de óxido de zinco.

Palavras-Chave: Óxido de Zinco; Nanopartículas; Mesoporoso; Síntese sol-gel;

Contents

Acknowledgments iii
Abstract iv
Resumo v
List of Tables viii
List of Figures x
Acronyms xii
Introduction 1
1.1. Zinc oxide nanoparticles 1
1.1.1. Preparation methodologies 2
1.1.2. Particle nucleation and growth theory 3
1.1.3. Key synthesis parameters 6
1.1.4. Mesoporous nanoparticles 9
1.2. Objectives 11
Experimental section 12
2.1 Materials 12
2.2 Equipment 12
2.3 Methods 13
Results and discussion 16
3.1 Sol-gel syntheses and characterization of ZnO NPs 16
3.2 Solvothermal synthesis and characterization of ZnO NPs 25
3.3 ZnO mesoporous nanoparticles 26
Conclusions 29
Future work 30
Bibliography 31

List of Tables

Table 1 - Experiments and corresponding synthesis parameters *14*
Table 2 - Results from SG1 and its repetition *16*
Table 3 - Results regarding the pH effect *17*
Table 4 - Results regarding the precursor concentration effect *20*
Table 5 - Results regarding the solvent effect *20*
Table 6 - Solvent properties *21*
Table 7 - Results regarding the influence of the reaction time *23*
Table 8 - Results regarding the influence of the reaction temperature *23*

List of Figures

Figure 1 - Schematic representation of the sol-gel process. 2
Figure 2 - Schematic representation of the nucleation process of ZnO crystal. 3
Figure 3 - Free energy diagram for nucleation explaining the existence of a "critical nucleus". 4
Figure 4 - Schematic diagram illustrating La Mer's condition for nucleation. 5
Figure 5 - Representation of electrostatic and steric stabilization between two nanoparticles. 6
Figure 6 - Sol-gel modified process for multifunctional MSNs. 10
Figure 7 - Schematic representation of sol-gel synthesis of ZnO NPs.. 13
Figure 8 - Schematic representation of solvothermal synthesis of ZnO NPs. 14
Figure 9 - A) TEM image of ZnO NPs synthesized by SG1 and B) Diameter distribution of ZnO NPs synthesized by SG1 17
Figure 10 – A) TEM image of ZnO NPs synthesized at pH 11 and B) Diameter distribution of ZnO NPs synthesized at pH 11 18
Figure 11 – TEM images (A and C) and diameter distribution (B and D) of ZnO NPs synthesized with a precursor concentration of 0.07M (A and B) and 0.13M (C and D). 19
Figure 12 - A) TEM image of ZnO NPs synthesized by solvothermal method and B) Diameter distribution of ZnO NPs synthesized by solvothermal method 21
Figure 13 - TEM images (A and C) and diameter distribution (B and D) of ZnO NPs synthesized in 0.5h (A and B) and 1h (C and D) 22
Figure 14 - TEM images (A and C) and diameter distribution (B and D) of ZnO NPs synthesized at 40˚C (A and B) and 60˚C (C and D). 24
Figure 15 - A) TEM image of ZnO NPs synthesized by solvothermal method and B) Diameter distribution of ZnO NPs synthesized by solvothermal method 25
Figure 16 - A) TEM images of the structures obtained by the Meso1 synthesis (A, B and C) and diameter distribution (D) 27
Figure 17 - TEM images of the structures obtained by Meso2 28

Acronyms

BET	Brunauer-Emmett-Teller
CTAB	Hexadecyltrimethylammonium Bromide
DEG	Diethylene Glycol
DLVO	Derjaguin-Landau-Verwey-Overbeek
HMT	Hexamethylenetetramine
LSW	Lifshitz– Slyozov–Wagner
MSN	Mesoporous Silica Nanoparticle
MZN	Mesoporous Zinc Oxide Nanoparticle
NPs	Nanoparticles
ROS	Reactive Oxygen Species
TEM	Transmission electron microscopy
TCO	Transparent Conductive Oxides
ZnO	Zinc Oxide

Chapter 1

Introduction

Zinc oxide (ZnO) is a metal oxide semiconductor that has aroused increasing interest from researchers in various fields of science. In nanotechnology, it has been extensively investigated due to its unique properties, such as relatively large exciton binding energy of about 60meV, direct wide band gap around 3.4eV, piezoelectricity, biocompatibility, low manufacturing cost, among others.[1] Such notable properties make it a very interesting material for a wide range of applications.

One of the most well-known applications is in optoelectronics. Zinc oxide belongs to the class of transparent conductive oxides (TCO) and its electrical properties, such as stability and high conductivity, electron affinity and mobility, combined with its optical properties, as exceptional ultraviolet absorbing properties and transparency for visible light, demonstrate its great potential for being used in optoelectronic devices (e.g. LEDs, laser diodes, solar cells, etc).[2][3]

ZnO nanoparticles (NPs) have also been extensively investigated for several biomedical applications. Due to their inherent ability to induce reactive oxygen species (ROS) generation and cause cell apoptosis, these nanoparticles are suitable for anticancer, antibacterial, and antifungal applications. They can also be loaded and administrated with other therapeutic agents, revealing potential for drug delivery applications, and their photo-luminescence properties make them applicable for biosensing applications and for the cosmetic sector, especially sunscreens.[4] Due to the antimicrobial and antibacterial properties, ZnO NPs are also commonly used in food packing and in the textile industry. [5][6][7]

In addition to the solar energy conversion applications, ZnO also fits into some other important applications in the environment sector. It can be used as gas sensor, since its surface conductivity can be strongly influenced by various gases, including some toxic and harmful ones like formaldehyde or nitrogen dioxide [8][9][10]). ZnO-based gas sensors have a rapid response, low detection limit, high selectivity, predictable performance and relatively low manufacturing cost.[11] It can also be used as photocatalyst, for example in the degradation of organic pollutants resistant to environment deterioration. For this purpose, its low-cost, non-toxicity and efficient absorption across a broad range of the solar spectrum have a significant importance.[12]

Besides the mentioned applications, ZnO is also used as an additive in many other industries (e.g. ceramics, paints, rubbers, coatings, adhesives, agriculture, etc).[13]

1.1. Zinc oxide nanoparticles

Nanomaterials can be defined as objects in which at least one of their dimensions is smaller than 100 nm, and depending on the overall shape, these materials can be from zero (0D) to three dimensions (3D). This class of materials has great potential since it has very particular physicochemical properties, which cannot be predicted from the bulk counterparts due to the quantum size effect and the high surface area to volume ratio.[14][15]

1.1.1. Preparation methodologies

Nanoparticles can be synthetized from two different approaches: the top-down approach and the bottom-up approach. The top-down approach is based on physical methods that transform larger materials into smaller nano-sized particles. Despite allowing the production of nanoparticles on an industrial scale, it does not allow such rigorous control of the sizes of the particles and their uniformity. In opposition, through the bottom-up approach it is possible to chemically synthesize particles with the desired shape and size, in a very controlled way.

Some examples of physical approaches to produce ZnO nanostructures include mechanical milling[16] or nanolithography techniques. [17][18] However as these methods are out of the scope of this thesis, they will not be discussed in further detail.

Chemical syntheses allow the control of matter from a molecular level which enables a better control of the particle size, shape, and size distribution. By understanding the correlation between how matter is assembled on an atomic level and the material macroscopic properties, it is possible to chemically design the syntheses methodology to achieve the desired products. Some chemical approaches to synthetize ZnO NPs include the sol-gel method[19][20], solvothermal method [21][22], co-precipitation[23][24], or biological green synthesis, which allows obtaining nanoparticles using microorganisms or plants. [25][26][6].

Sol-gel is one of the most versatile methods used to produce different nanomaterials, especially metal oxide nanoparticles. This method is very simple and cost effective, allows a great control of the size, porosity and morphology of the nanoparticles, it easily allows chemical doping and surface modification, and can be carried out at room temperature. For these reasons sol-gel is an efficient technique to produce high quality products, and thus it was the main used technique in this thesis.

In this technique, a precursor is primarily hydrolysed, originating a colloidal solution (sol), which after polycondensation forms a gel-like substance (gel). After aging, the gel is dried, and the final nanostructures are obtained. In some cases, it may be justified to apply a thermal treatment/calcination to the product obtained [27][28][29] (Figure 1).

One of the most used zinc source precursors is zinc acetate dihydrate, although there are references to others, such as zinc chloride or zinc nitrate. Sodium hydroxide is also one of the most reported hydrolysing agents and pH controllers for these syntheses, but it is also possible to find cases where other bases are used, such as ammonium hydroxide or potassium hydroxide.[30][31][32]

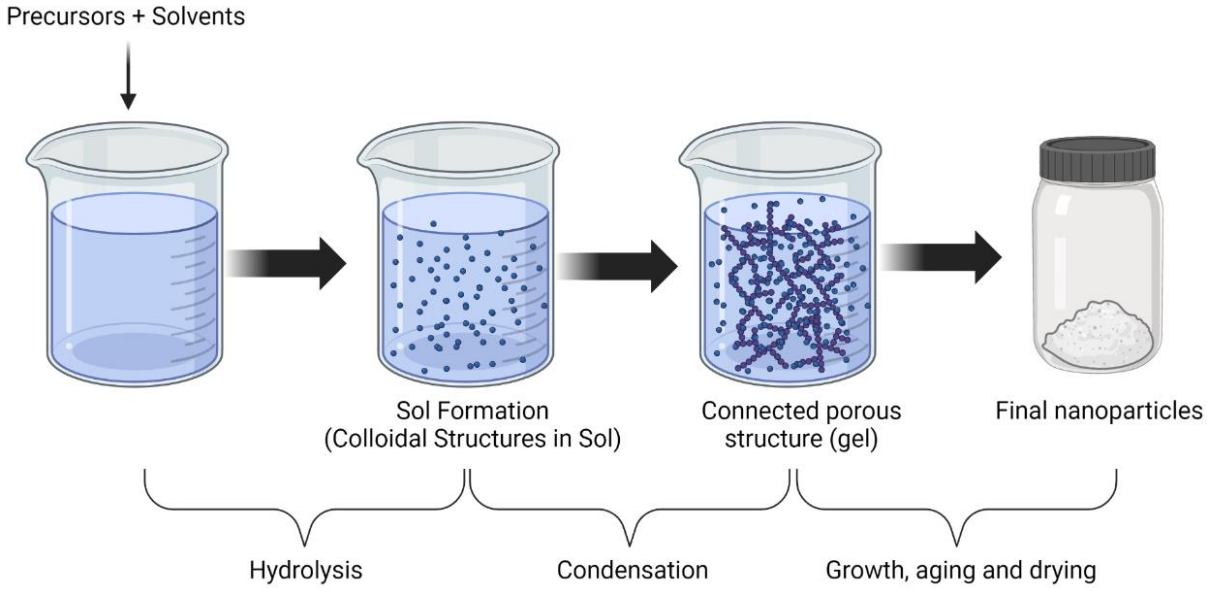

Figure 1 - Schematic representation of the sol-gel process. Created in BioRender, adapted from [27]

1.1.2. Particle nucleation and growth theory

The sol-gel synthesis can be divided in four steps: (i) hydrolysis, (ii) condensation and polymerization (nucleation) of monomers to form particles, (iii) growth of particles, and (iv) aging.

The chemical reactions involved in the formation of ZnO whose initial precursor is zinc acetate dihydrate [$Zn(CH_3COO)_2 \cdot 2H_2O$] and in which is used sodium hydroxide ($NaOH$) as a hydrolysing agent and pH controller, can be described by Equations 1 – 3: [33]

$$Zn(CH_3COO)_2 \cdot 2H_2O + 2NaOH \rightarrow Zn(OH)_2 + 2CH_3COONa + 2H_2O \quad (1)$$

$$Zn(OH)_2 + 2H_2O \rightarrow Zn(OH)_4^{2-} + 2H^+ \quad (2)$$

$$Zn(OH)_4^{2-} \rightarrow ZnO + H_2O + 2OH^- \quad (3)$$

Initially, the solution of $Zn(CH_3COO)_2 \cdot 2H_2O$ reacts with $NaOH$ to form zinc hydroxide $Zn(OH)_2$, sodium acetate (CH_3COONa) and water molecules (H_2O), (Equation 1). $Zn(OH)_2$ reacts with water to form the growth unit $Zn(OH)_4^{2-}$ and hydrogen ions (H^+), (Equation 2). Lastly, the ZnO precipitates through condensation reaction (Equation 3), in which the $Zn(OH)_4^{2-}$ ions are adsorbed onto the ZnO crystal particles[33][34].

The schematic diagram of the nucleation process can be represented as follows:

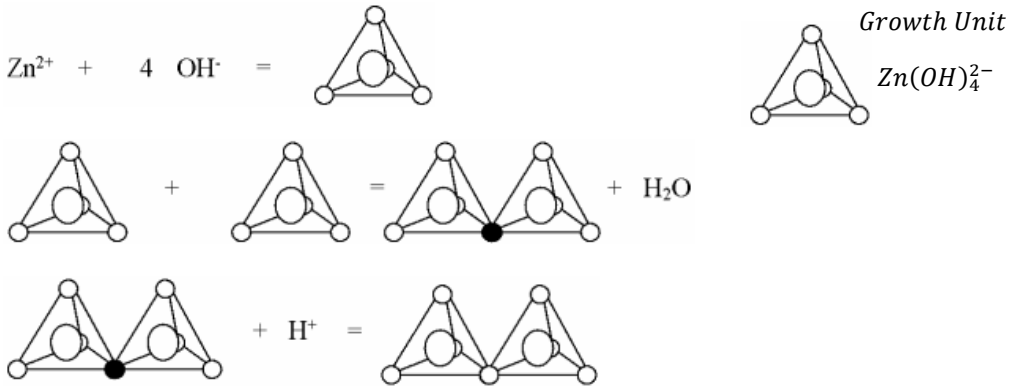

Figure 2 - Schematic representation of the nucleation process of ZnO crystal. Reproduced from [35]

Nucleation can be categorized as homogeneous or heterogeneous. In homogeneous nucleation, the solute molecules combine to produce nuclei in the absence of an interface since the supersaturated solution is not thermodynamically stable [14][36]. In this process, the total free energy (ΔG_T) is defined as the sum of the surface free energy (ΔG_S) and the bulk free energy (ΔG_V) (Equation 4). For spherical particles of radius r, with surface energy γ, and free energy of the bulk crystal Δg_V, the total free energy can be represented by: [36]

$$\Delta G_T = \Delta G_S + \Delta G_V = 4\pi r^2\gamma + \frac{4}{3}\pi r^3 \Delta g_V \quad (4)$$

The crystal free energy depends on temperature T, Boltzmann's constant k_B,the supersaturation of the solution S, given by c_1/c_s , with $c_1$the precursor concentration and c_s the solubility of the solid phase, and its molar volume v, being described by: [36]

$$\Delta g_V = \frac{-k_B T \ln(S)}{v} \tag{5}$$

The surface free energy is always positive, and the crystal free energy is always negative. The corresponding sum originate a curve with a maximum free energy value (Figure 3). This value corresponds to the critical free energy and can be obtained by differentiating ΔG_T with respect to r, and setting it to zero, $\mathrm{d}(\Delta G_T)/r = 0$: [36]

$$\Delta G_{crit} = \frac{4}{3}\pi\gamma r_{crit}^2 \tag{6}$$

The critical radius corresponds to the minimum size at which a particle can remain in the solution without being redissolved, as defined by: [36]

$$r_{crit} = \frac{-2\gamma}{\Delta G_V} = \frac{2\gamma v}{k_B T \ln(S)} \tag{7}$$

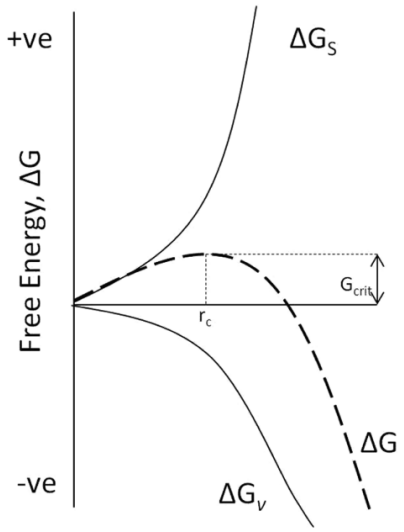

Figure 3 - Free energy diagram for nucleation explaining the existence of a "critical nucleus". Taken from [36]

The nucleation rate, J_N, can be expressed in terms of ΔG_{crit} and a pre-factor, J_0 : [36]

$$J_N = J_0 \exp\left(-\frac{\Delta G_{crit}}{k_B T}\right) = J_0 \exp\left(\frac{-16\pi v^2\gamma^3}{3(k_B T)^3(\ln S)^2}\right) \tag{8}$$

In heterogeneous nucleation, unlike homogeneous nucleation, the nuclei are formed on foreign bodies, such as surfaces or impurities. In their presence, the energy barrier to overcome for nucleation decreases since the surface energy is much lower.[36]

For several years, the process of nucleation and growth of nanoparticles have been explained through the LaMer burst nucleation, followed by Ostwald ripening to describe the variation in the particles size. According to the LaMer plot for the crystal nucleation process (Figure 4), when the concentration of solute increases as a function of time, no nucleation would occur even above the equilibrium solubility. It is necessary to achieve a specific value of supersaturation, above the solubility value, for the nucleation to occur. This value corresponds to the critical energy barrier for the formation of nuclei (Equation 6).

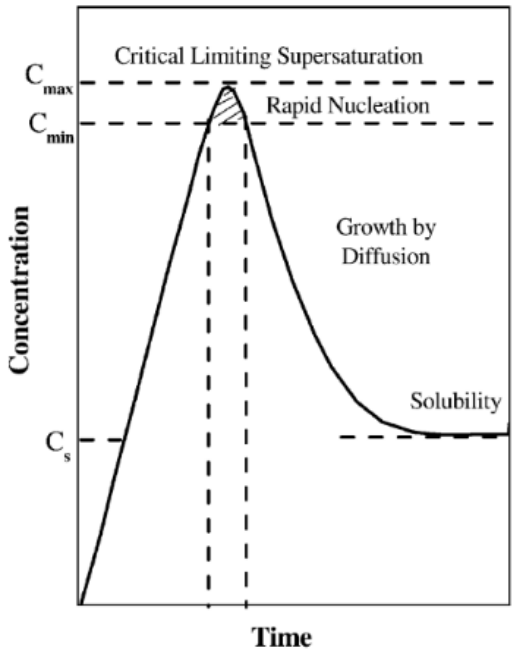

Figure 4 - Schematic diagram illustrating La Mer's condition for nucleation. Taken from [37]

Once nucleation starts, growth occurs simultaneously, although these two processes proceed at different speeds. From the moment nuclei are formed, the concentration of solute decreases as does the change of Gibbs free energy. When the concentration decreases below this specific value, which corresponds to the critical energy, no more nuclei would form, whereas the growth will proceed until the precursor concentration has equilibrated with the metal oxide, which is determined by solubility.[38]

After nucleation and growth, the particles sizes can vary due to aging processes, during which the total amount of solid material remains constant. The two main processes are Ostwald ripening (or coarsening) and aggregation.[39]

According to the classical Ostwald ripening mechanism, smaller particles redissolve due to their high surface energy, allowing larger particles to grow. This process, driven by the reduction of the surface energy, was quantified by Lifshitz and Slyozov and then followed by Wagner, and is known as the LSW theory.[36]

Aggregation is a process that involves the formation and growth of clusters and is controlled by both interfacial chemical reactions and particle transport mechanisms. According to the DLVO theory, a colloidal system is stable when the repulsive forces overcome the attractive forces. Some approaches to decrease the aggregation and stabilize a colloidal system and increase the repulsive forces include increasing the particle size or the zeta potential. Another way to achieve colloidal stabilization is through steric repulsion, in which polymeric molecules, adsorbed on the surface of the nanoparticles, increase the repulsive forces [40] (Figure 5).

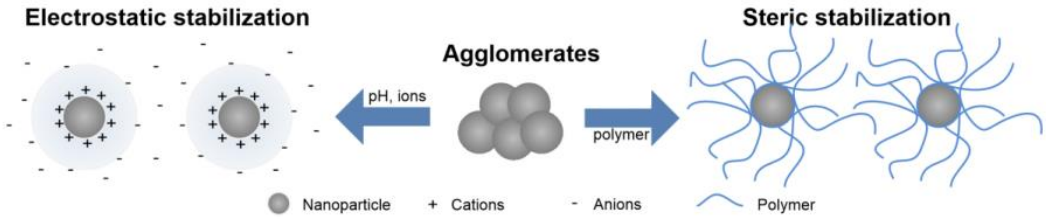

Figure 5 - Representation of electrostatic and steric stabilization between two nanoparticles. Taken from [41]

The mechanism of nucleation, growth and aging of nanoparticles is a complex area of intense interest. There are more theories that try to explain those mechanisms, such as Finke-Watzky two step mechanism, digestive ripening, coalescence, orientated attachment or interparticle growth.[36]

The presented theory provides a basic summary of how to control particles formation within solution by revealing some key controllable parameters, nevertheless, the nucleation and growth of each material depends on its reaction conditions and small changes can lead to different mechanisms.[36]

1.1.3. Key synthesis parameters

The synthesis of zinc oxide nanoparticles is strongly affected by the external conditions such as pH of the solution, precursor concentration, reaction time and temperature or the solvent used. Therefore, the control of the synthesis parameters is essential to obtain the desired set of characteristics in the final nanoparticles.

1.1.3.1. Effect of pH

The pH of the solution is a critical factor in the sol-gel syntheses of ZnO nanoparticles. The amount of H^+ or OH^- ions affects the hydrolysis and condensation stages. It can determine the number of ZnO nuclei and growth units.[33] According to Equations 1 – 3, the OH^- ions allow the formation of the growth unit $Zn(OH)_4^{2-}$, which promotes the nucleation and growth of the ZnO NPs. Therefore, alkaline sol pH values should favour the particles formation reactions.

Alias et al.[33] studied the effect of pH, from 6 to 11, on the properties of ZnO NPs synthetized by sol-gel method. This experiment was carried out at room temperature, using zinc acetate dihydrate as zinc source, sodium hydroxide as pH regulator and methanol as solvent. It was verified an inability to form ZnO in acidic and neutral mediums (pH=6 and 7) due to the lack of OH^- ions. The X-ray diffraction analysis at these two pH values did not show any intense ZnO peaks, contrary to the remaining results (pH=8, 9, 10 and 11). By increasing the pH of the solution from 8 to 11, it was reported a decrease in the particle size (50 to 37 nm) and in the energy band gap value (3.25 to 3.14 eV). However, at higher OH^- concentrations (pH ≥ 10), the OH^- ions react with ZnO originating $Zn(OH)_4^{2-}$(Equation 3 – inverse reaction) leading to the dissolution of ZnO, which originates smaller and more agglomerated ZnO NPs. The authors concluded that the best morphological and optical properties were obtained at pH 9, with uniform and spherical particles.

In another experiment, Wahab et al.[42] studied the role of pH variation on the growth of zinc oxide nanostructures. Zinc acetate dehydrated and sodium hydroxide were also used, but with different concentrations. This procedure is different from the above because distilled water was used as solvent and the pH adjustment was made using NaOH and HCl solutions. After the pH adjustment, the solutions were refluxed for 1 hour at 90ºC. Samples with pH values from 6 to 12 were analysed and the results showed that for all the cases, the X-ray diffraction peaks matched with ZnO pattern, meaning that ZnO nanostructures were obtained, unlike the previous article. The SEM and TEM images showed that for acidic and neutral mediums, sheet-like structures were obtained and an increase in pH values revealed a shift towards flower-like structures composed of sharp tipped nanorods. According to the authors, the

pH influences the structure of the zinc oxide nanostructures. In acidic medium solutions, the higher amount of H^+ ions inhibit the hydrolysis and condensation processes, leading to smaller aggregates. The H^+ ions react preferentially with OH^- ions at the surface of zinc oxide nanostructures, inhibiting their growth in certain directions. In basic solutions, OH^- ions are strongly attracted by the positively charged Zn-terminated surfaces. In this article, particle sizes and band gap values were not discussed or presented.

Li et al.[35] studied the role of the pH as well on the particle morphology and size, however under hydrothermal conditions. Zinc acetate dehydrated and sodium hydroxide were also used as starting materials. Like the previous paper, distilled water was used as solvent and the pH adjustment was made using NaOH and HCl solutions. The reactions proceeded in a Teflon-lined stainless-steel autoclave at 200ºC for 12h. Three pH values were analysed (pH = 5, 7 and 11). The results obtained confirmed that the higher the pH value, the smaller the particle size (7700, 1200 and 530 nm). The morphology also changed from a slice-like structure in acidic medium to a prism-like structure in basic medium. In this paper, the authors reported with more detail the role of the H^+ ion in the synthesis mechanism of ZnO nanoparticles. According to them, although the H^+ ion prevents the formation of the growth unit, it has a role in protonating the structure resulting from the oxolation reaction of the growth units (Figure 2), and as such, these conditions must be also considered in consideration when discussing the effect of the pH value on ZnO NPs syntheses. Nevertheless, this subject was not discussed in more detail.

1.1.3.2. Precursor concentration

The precursor concentration has a direct influence on the nucleation step, specifically on the nucleation rate, and consequently, on the number and size of the nanoparticles. According to Equation 8, the nucleation rate is expected to decrease strongly with increasing supersaturation. The supersaturation is given by c_1/c_s, with $c_1$the precursor concentration and c_s the solubility of the solid phase. Therefore, the nucleation rate will be higher when the precursor concentration is higher, and the solid phase solubility is lower.[43][44]

Higher nucleation rates produce more nuclei, which tend to form smaller particles. However, the precursor concentration may also influence the coarsening rate, which also affects the final particle size. Oskam et al.[43] studied the influence of some experimental parameters, including the precursor concentration, on the coarsening kinetics of ZnO nanoparticles. In this study, ZnO nanoparticles were synthesized from $ZnCl_2$ and NaOH in ethanol, using solutions with different precursor concentrations (1 mM, 14 mM, and 100 mM). The main results showed that the particle coarsening rate was the same for the 1 mM and 14 mM solutions, with a significantly faster increase for 100 mM. According to the authors, the coarsening rate is independent of precursor concentration up to a threshold concentration, however, at sufficiently high concentrations, the inter-particle distance is small enough to facilitate faster coarsening. No images of the nanoparticles were shown in the article, nor detailed values for size or energy band gap.

Although the impact of the precursor concentration seems to be more relevant to the nucleation rate, these results strengthen the hypothesis that the influence of a given parameter may not be as linear or predictable as expected.

1.1.3.3. Solvent

Solvent choice is an important parameter that influences the nucleation, growth, and aggregation rate of a ZnO NPs synthesis.

The polarity and dielectric constant of the solvent are two major factors that affect the growth mechanism. Their role can be explained by the electrostatic force that is decisive in the growth mechanism of ZnO NPs. The repulsive electrostatic interaction energy between 2 particles is given by: [45]

$$E = \frac{1}{4\pi\varepsilon}\frac{Q_1 Q_2}{r} \quad (9)$$

where ε is the dielectric constant of the medium, Q_1 and Q_2 are the charge values of the two particles and r is the separation between two particles. This repulsive force hinders particle aggregation and consequently leads to a decrease in the growth rate. This interaction energy is directly proportional to the charge value of the ZnO nanoparticles and is inversely proportional to the dielectric constant of the solvent molecules. The charge value of ZnO nanoparticles is derived from the ionization of the solvent molecules, which is intimately related to its polarity. Therefore, the ZnO growth behaviour depends directly on the polarity and inversely on the dielectric constant of solvent molecules.[45]

Hu et al.[45] studied the influence of the solvent on the growth of these nanoparticles. ZnO nanoparticles were synthesized by precipitation from solution at temperatures between 30 and 65ºC, using zinc acetate dehydrated and sodium hydroxide as starting materials, and ethanol, 1-propanol, 1-butanol, 1-pentanol and 1-hexanol as solvents. The obtained particles had sizes between 1 and 7 nm, depending on the reaction time and temperature and on the solvents used, and presented spherical shape. The results showed that for longer chain length alcohols, i.e. for weaker polar solvents with a lower dielectric constant, the nucleation and growth rates are faster compared to shorter chain length solvents.

After nucleation and growth were completed, the particle size increased with time by coarsening. The coarsening kinetics were consistent with the LSW model, whose rate law is given by: [46]

$$\bar{r}^3 - \bar{r_0}^3 = kt \quad (10)$$

where $\bar{r}$ is the average particle radius, $\bar{r_0}$ is the average initial particle radius, k is the rate constant, and t is time. The coarsening rate constant is given by: [46]

$$k = \frac{8\gamma D \nu c_{r=\infty}}{9RT} \quad (11)$$

where γ is the surface energy, D is the diffusion coefficient, defined by the Stokes-Einstein equation (Equation 12) [46], ν is the molar volume, and $c_{r=\infty}$ is the equilibrium concentration at a flat surface, i.e. the bulk solubility. Substituting the diffusion coefficient from Stokes-Einstein equation, the rate constant can be expressed by Equation 13 [46]:

$$D = \frac{k_B T}{6\pi\eta a} \quad (12)$$

$$k = \frac{8\gamma \nu^2 c_{r=\infty}}{54\pi\eta a N_A} \quad (13)$$

where $k_B$is the Boltzmann constant, $k_B = R/N_A$, η is the viscosity of the solvent and a is the solvated ion radius. Therefore, the choice of solvent seems to not only influence the nucleation and growth rates, but also the coarsening rate.

In a similar experiment, Ramya et al.[47] synthesized ZnO nanoparticles by integrating a simple solution method with ultrasonication. In this synthesis, zinc acetate dihydrate and sodium hydroxide solutions were mixed under ultrasonication for 10 minutes. The solution was then heated at 80°C for 2

hours. Methanol, ethanol, 1-butanol, 1-hexanol, 1-octanol and 1-decanol were the solvents used in this study. Unlike the previous experiment, two types of morphologies were obtained, spherical and rod-like. The particle sizes are between 17 and 27 nm, for the diameter, and 17 and 90 nm, for the length. Methanol and 1-decanol samples showed nanodot structures with small and larger particles sizes respectively. Samples 1-butanol and 1-hexanol consist of dispersed nanorods with increasing length with respect to the alkyl group length of the solvent. Ethanol and 1-octanol samples correspond to the transition states from nanodots to nanorods and vice-versa. According to the authors, the number of -CH_2 bonds affects the polarity, viscosity and solvency of the alcohol, which greatly influences the growth rate of the nanostructures. In strong polar solvents, like methanol, the growth rate experienced is slower, justifying the obtained spherical morphology. When the alkyl group length increases, the growth rate increases, just like the length of the rods. In 1-decanol, the particles assumed a dot like structure again. The authors justify this result with its high zeta potential value. Zeta potential decreases with an increase in the alkyl group length of the solvent, however for 1-decanol, an increase was noticed. An increase in the zeta potential increases the electrostatic repulsive force between the nanoparticles, which results in slow growth kinetics.

1.1.3.4. Reaction temperature and time

The reaction temperature has a direct influence on the nucleation step, specifically on the nucleation rate and consequently on the number and size of the nanoparticles. According to Equation 8, the nucleation rate is expected to decrease strongly with increasing temperature. As already mentioned, the smaller the number of nuclei, the larger will tend to be the final particle size.

According to Hu et al.[46] (in the experiment previously mentioned in 1.2.3.3.), nucleation and growth are relatively fast, and at longer times, the average particle size continues to increase due to coarsening mechanisms. This result is coherent with Equation 10. For all the solvents tested, the coarsening rate also increased with an increase in temperature. Although the coarsening rate constant does not depend directly on temperature (Equation 13), temperature is a factor that ends up influencing other determining parameters such as viscosity or surface energy. An increase in temperature tends to decrease the viscosity and the surface energy. A decrease in the solvent viscosity contributes to an increase of the coarsening rate constant. However, a decrease in the surface energy has the opposite effect. Therefore, during coarsening, an increase in temperature may be simultaneously contributing, through different parameters, to the increase and decrease in particle size. According to the results of this experiment, the effect that contributes to the particle size increase prevails.

There are many factors that have a direct or indirect influence on the synthesis of ZnO nanoparticles and it is difficult to predict how they affect it, since many of them interfere in different ways. However, this introduction serves as a guide to try to better understand the mechanisms involved in these syntheses in order to obtain a final product with the desired characteristics.

1.1.4. Mesoporous nanoparticles

According to IUPAC, mesoporous nanoparticles correspond to those whose pore sizes are in the range between 2 and 50 nm.[48] These nanoparticles have attracted great interest due to their specific structures and properties. The large surface/volume ratio, high porosity and low density make porous nanoparticles suitable for several potential applications, such as magnetic resonance imaging, catalysis, separation, gas sensor, and drug delivery, being the last one of the most promising.[49]

Mesoporous silica nanoparticles (MSNs) are one of the most well-studied inorganic nanoparticles for drug delivery and contrast agents. The NPs have a good compatibility, and their synthesis is simple, versatile, low cost and scalable. These nanoparticles can be obtained with a well-defined particle morphology with diameters from 40 nm to hundreds of nanometres, adjustable pore size from 2 to 8 nm in diameter, ordered geometry and very high internal surface area and pore volume.[50]

Their versatile synthesis process (Figure 6) makes it possible to obtain a wide variety of structures that can be functionalized in different ways, allowing the creation of smart delivery systems, with the possibility of accommodating large drug loads, be traceable and feature targeting and smart release control mechanisms that allow the delivery of the cargo at the desired location.[51]

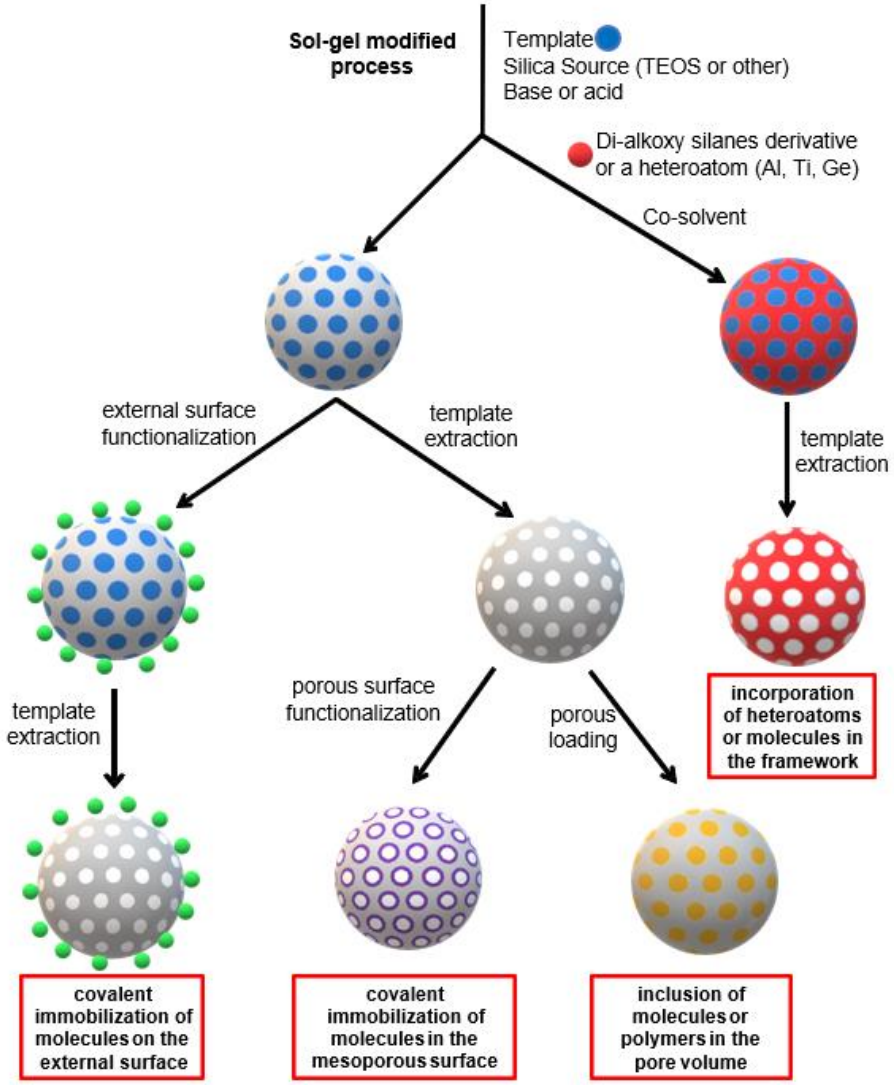

Figure 6 - Sol-gel modified process for multifunctional MSNs. Taken from [52]

Mesoporous zinc oxide nanoparticles are a far less developed field of study than MSNs, but there are some first approaches published on mesoporous zinc oxide nanoparticles (MZNs). Lu et al.[53] synthesized nanosheet-based ZnO microspheres with porous nano-structures by a facile chemical bath deposition method followed by thermal treatment, which was investigated to build electrochemical biosensors. The microspheres showed a sponge-like pore structure, whose cavities sizes is about several hundred nanometers. The thickness of the nanosheets is about 20nm. The hydrothermal synthesis can be summarized by the reaction of zinc nitrate hexahydrate and hexamethylenetetramine (HMT) in water, with trisodium citrate serving as a structure-modifying agent. It was proposed that HMT reacts with water to produce ammonia, which in turn reacts with water to produce OH- anions. The microspheres obtained after 1 hour of reaction are monodispersed and around 1 µm in diameter. They are composed of randomly growing nanosheets, connected with each other, with thicknesses in the range between 10 and 20 nm. According to the authors, the nanosheets could correspond to a hydrated form of amorphous ZnO.

Bakrudeen et al.[54] prepared spheroidal mesoporous auto-fluorescent ZnO nanospheres by modified continuous distillation method for drug delivery carrier applications. In this synthesis zinc acetate dihydrate was added into ethanol and the solution was refluxed for 90mins at 80ºC. It was further placed in an ice bath at 0ºC and lithium hydroxide was slowly added under ultra-sonication. Lastly, the solution was stirred for 1h at 30-35ºC. The particles were spherical in shape, with sizes ranging between 65 and 121nm, and average pore size of 4nm. Despite the claimed results, it is difficult to confirm mesoporosity by the images presented.

Barick et al.[49] fabricated highly mesoporous spherical 3D ZnO nanoassemblies by a facile soft-chemical approach also for drug delivery applications. Zinc acetate was heated under reflux in diethylene glycol (DEG) medium and ZnO nanocrystals were precipitated out shortly after reaching 160-165ºC. The results showed that the spherical porous assemblies obtained (broad size range: 100–600 nm) are comprised of numerous nanocrystals of 20 nm, on average, with an average pore diameter size of 28nm.

Although these methods represent first approaches to synthesizing mesoporous zinc oxide nanoparticles, there are still no scalable versatile syntheses yielding well-defined morphologies with reduced pore and particle sizes.

1.2. Objectives

The aim of this work is to understand the growth mechanism of zinc oxide nanoparticles by sol-gel method, and how their synthesis parameters affect their final structure, namely their morphology and size. Although there are some articles on the influence of certain synthesis parameters on the characteristics of zinc oxide nanoparticles, their role is still not clear, and the information available is sometimes contradictory.

A second objective of this work is to develop mesoporous zinc oxide nanoparticles by the sol-gel method. Zinc oxide is a material whose interest has been increasing in recent times and if it is possible to combine it into a mesoporous nanostructure, it could add value to currently existing mesoporous nanoparticles, due to its unique optical properties. It could also be of great interest for drug delivery applications for example.

Currently there are no well-developed syntheses that allow obtaining stable mesoporous ZnO NPs with well-defined morphologies. This thesis provides a starting point for the investigation of this specific type of particles and for the understanding of the growth mechanism of ZnO nanoparticles.

Chapter 2

Experimental section

2.1 Materials

For the sol-gel syntheses of ZnO nanoparticles, the following materials were used: zinc acetate dihydrate ([$Zn(CH_3COO)_2 \cdot 2H_2O$], ≥ 98%, Sigma-Aldrich) as zinc source, sodium hydroxide (pure NaOH, pellets, PanReac AppliChem) as hydrolysing agent and pH controller, and absolute methanol (MeOH, ≥99.9%, Riedel-de Haën), and deionized water (produced from a Millipore system Milli-Q ≥18 MΩcm with a Millipak membrane filter 0.22 µm) as solvents.

Absolute ethanol (EtOH, ≥99.8%, Riedel-de Haën) was used as solvent in the solvothermal and mesoporous syntheses. It was also used to wash the particles and disperse them before the TEM images.

For the synthesis of mesoporous nanoparticles an ammonium hydroxide solution (~25% NH_3 basis, Sigma-Aldrich) was also utilized and hexadecyltrimethylammonium bromide (CTAB, ≥99%, Sigma) was used as cationic surfactant.

2.2 Equipment

2.2.1 Centrifuge

The nanoparticles were centrifuged using a Sigma 2k15, with a 12141 rotor, at 19890 g and 20ºC. The polypropylene tubes used had a volume capacity of 10 mL.

The centrifugations of the mesoporous nanoparticles were carried on a Beckman Coulter, model Avanti J30I at 30 000 and 80 000 g at 20ºC. The polypropylene tubes used had a volume capacity of 40 mL.

2.2.2 Transmission electron microscopy (TEM)

A Hitachi transmission electron microscope, model H-8100, equipped with a 200kw accelerator voltage and a LaB_6 filament was used to obtain the TEM images of the nanoparticles. The images were digitally acquired with a KeenView camera (Soft Imaging System) incorporated in the microscope. The samples for analysis were prepared by dispersing the nanoparticles in ethanol and dipping a copper grid coated with carbon in the dispersion, which was then left to air dry. The software ImageJ was used to analyse and estimate the size, shape factor (n) and morphology of the nanoparticles by evaluating at least 50 nanoparticles in each image.

The shape factor (n) corresponds to the ratio of the Feret diameter (farthest possible distance between the two parallel tangents of an object) with the minimum Feret diameter of the particle (closest possible distance between the two parallel tangents of an object) (Equation 14). This parameter allows the evaluation of the shape of the nanoparticles. The closest the shape factor is to 1, the more spherical are the particles[55].

$$n = \frac{Feret\ Diameter}{Minimum\ Feret\ Diameter} \quad (14)$$

2.3 Methods

2.3.1 Sol-gel syntheses of Zinc Oxide Nanoparticles

ZnO nanoparticles were prepared by sol-gel methods. Initially a control synthesis (*SG1*) was defined, based on some research articles[33][34]:

SG1 (control)

ZnO sol was prepared by adding 1g of zinc acetate dihydrate under magnetic stirring into 23 mL of methanol (0.2M), at room temperature, until a clear solution was obtained (5 min proved to be enough). Then, a 5M sodium hydroxide solution (in methanol) was added drop-by-drop to adjust the pH value of the solution to 9. The resulting milky white gel was kept under stable stirring for another 2h and 30min. After that, the dispersion was centrifuged (19890 g, 15mins) and washed 3 times with absolute ethanol. In the last cycle, the supernatant was removed, and the nanoparticles were dried at 50 °C in a ventilated oven. Figure 7 corresponds to a representation of the mentioned synthesis.

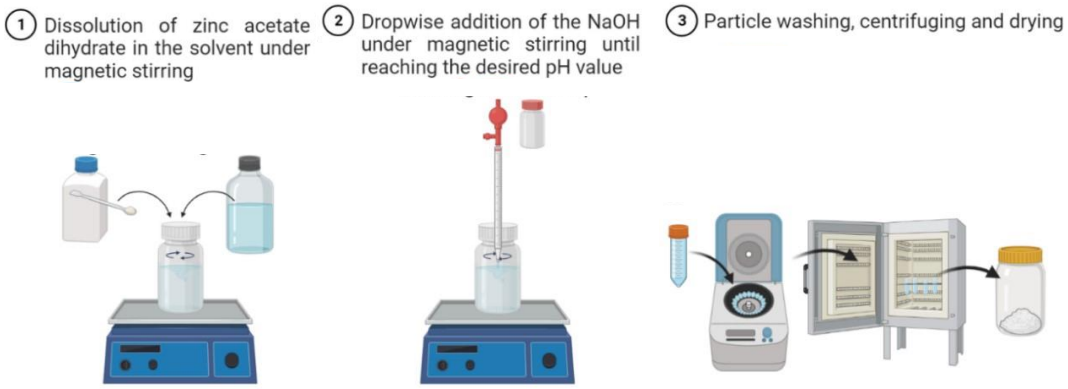

Figure 7 - Schematic representation of sol-gel synthesis of ZnO NPs. Created with BioRender.

Subsequent changes were made to the synthesis parameters in order to understand their influence on the characteristics of the final particles. In *SG2* and *SG3* the pH values of the solutions were changed to 7 and 11, respectively. In *SG4* and *SG5* the initial precursor concentration was changed to one-third and two-thirds of the control experiment value. In *SG6* the solvent used was water. *SG7* and *SG8* introduce variations in reaction time to 30min and 1h, respectively. Finally, in *SG9* and *SG10* the reactions were carried out at 40 and 60ºC, respectively. The syntheses carried out are summarized in Table 1.

Table 1 - Experiments and corresponding synthesis parameters

Experiment	pH value	Temperature (ºC)	Precursor concentration (M)	Solvent	Reaction time (h)
SG1	9	Room Temp.	0.2	MeOH	2.5
SG2	7	Room Temp.	0.2	MeOH	2.5
SG3	11	Room Temp.	0.2	MeOH	2.5
SG4	9	Room Temp.	0.07	MeOH	2.5
SG5	9	Room Temp.	0.13	MeOH	2.5
SG6	9	Room Temp.	0.07	H_2O	2.5
SG7	9	Room Temp.	0.2	MeOH	0.5
SG8	9	Room Temp.	0.2	MeOH	1
SG9	9	40	0.2	MeOH	2.5
SG10	9	60	0.2	MeOH	2.5

2.3.2 Solvothermal synthesis of zinc oxide nanoparticles

The solvothermal synthesis (henceforth referred to as *ST* experiment) was carried out as described by Achouri et al.[56]. In a polypropylene bottle 511 mg of zinc acetate dihydrate were dissolved in 35 mL of ethanol under magnetic stirring. A NaOH solution (96 mg NaOH in 35 mL ethanol) was added dropwise and the mixture was stirred at room temperature for 30 min. Then, the solution was transferred into a 140 mL Teflon-sealed autoclave and was heated at 160 °C for 24 h. After cooling, the dispersion was centrifuged (19890 g, 15mins), washed 3 times with water, one with absolute ethanol, and dried at 70 °C overnight, as represented by Figure 8.

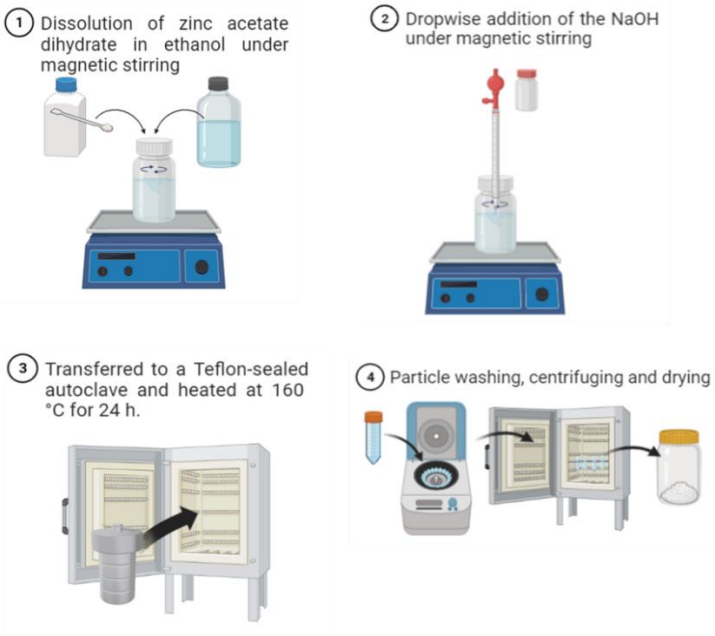

Figure 8 - Schematic representation of solvothermal synthesis of ZnO NPs. Created with BioRender.

2.3.3 Syntheses of mesoporous zinc oxide nanoparticles

The performed syntheses were based on successful and well-developed syntheses of mesoporous silica nanoparticles. Their methods and precursors were adapted in order to obtain zinc oxide mesoporous nanoparticles. Two main syntheses were carried out: *Meso1* and *Meso2*.

Meso 1

Meso1 was adapted from the work described by Ribeiro et al.[57]. First, 0,5 g of CTAB were dissolved in 230 mL of water at 32ºC, under stable magnetic stirring. After the temperature has stabilized, 1,75 mL of a 1.5M NaOH solution (in water) was added. After 30 min, 10 mL of an as prepared 1.1M zinc acetate dihydrate solution (in water) was carefully added dropwise to the solution. The reaction proceeded for 3 h and then the dispersion was centrifuged (80000 g, 15mins) and washed 2 times with distilled water and 2 times with absolute ethanol. In the last cycle, the supernatant was removed, and the nanoparticles were dried at 50 °C in a ventilated oven.

Meso2

Meso2 was adapted from the work described by Rodrigues et al.[58]. Initially 0,113 g of CTAB were dissolved in 58,7 mL of an as prepared 0.5M ammonium hydroxide solution (in water) at 50ºC, under stable magnetic stirring. After 30 min, 12,2 mL of a 0.15M zinc acetate dihydrate solution (in ethanol) was added dropwise to the solution. The reaction proceeded for 6 h and then the solution was left to age in a ventilated oven at 50ºC for 24h. After cooling, the dispersion was centrifuged (30000 G, 20 minutes) and washed 2 times with a mixture of 1:1 water/ethanol and 3 times with only absolute ethanol. In the last cycle, the supernatant was removed, and the nanoparticles dried at 50 °C in a ventilated oven.

Chapter 3

Results and discussion

In this chapter, the results regarding the influence of synthesis parameters on simple zinc oxide nanoparticles are firstly analysed (*SG1 – SG10*). It is discussed how these parameters affect the final structure of the particles synthesized by the sol-gel method, namely their morphology and size, and if these results are in line with what is expected and with was discussed in the literature. Then, a comparison is made between the results of sol-gel syntheses with those obtained by a solvothermal synthesis (*ST*), with a reflection on the best method to adopt. Finally, the results of the mesoporous syntheses (*Meso1* and *Meso2*) are discussed, and their relevance and feasibility are evaluated.

3.1 Sol-gel syntheses and characterization of ZnO NPs

As previously described, ZnO NPs were synthesized using a sol-gel method. The first synthesis (*SG1*) was performed to understand the process, and subsequently repeated to optimize the different parameters. Despite having a few differences, it was adapted from published syntheses whose results appeared to present relatively stable particles with good physical characteristics (e.g. articles developed in [33] or [34]). *SG1* was defined as the control synthesis and was performed at pH=9, during 2h30, at room temperature, with an initial precursor concentration of 0.2M and methanol as solvent. Syntheses *SG2-SG10* have the same base procedure as *SG1*, with a synthesis parameter being varied to analyse its influence on the final nanoparticles.

The obtained nanoparticles were analysed by TEM to estimate their average diameter and shape factor (n). Figure 9 shows the TEM image and diameter distribution analysis of *SG1*.

The average diameter of the ZnO NPs obtained for *SG1* was 8 ± 1 nm with an average shape factor of 1,2 ± 0,2. The *SG1* procedure was repeated and proved to be reproducible, as shown by the results in Table 2. Both syntheses presented particles with very similar sizes and almost spherical.

The reaction yield obtained for this synthesis was about 88%. In all experiments, the reaction yield was determined through the ratio between the obtained mass of ZnO and the expected mass of ZnO. The expected mass of ZnO was calculated assuming that the number of moles of the initial zinc precursor is equal to the number of moles of ZnO (Equations 1-3).

Table 2 - Results from SG1 and its repetition

Experiment	Average particle diameter (nm)	Average shape factor
SG1 (control)	8 ± 1	1,2 ± 0,2
SG1 (repetition)	9 ± 1	1,1 ± 0,1

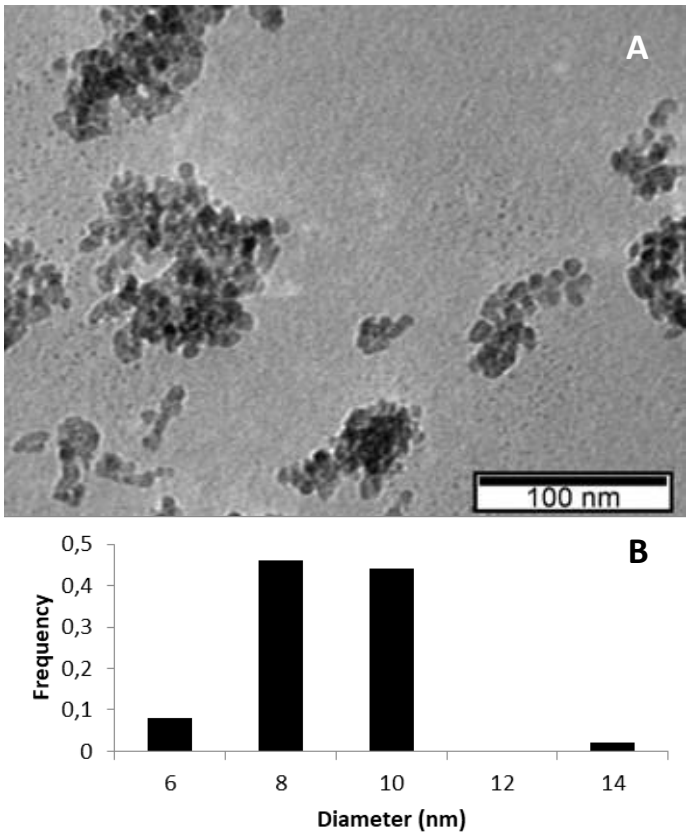

Figure 9 - A) TEM image of ZnO NPs synthesized by SG1 and B) Diameter distribution of ZnO NPs synthesized by SG1

3.1.1 Influence of the pH

In order to understand the pH effect on the size of the final nanoparticles, the pH value of the solution was changed while the remaining conditions were kept constant (precursor concentration, solvent, reaction time and temperature). *SG2* and *SG3* tested pH values of 7 and 11 respectively.

In *SG2* it was not possible to obtain particles during the centrifugation stage, and therefore no TEM images were taken. In the control synthesis, when NaOH is added to the solution, the resulting mixture becomes opaque and takes on a milky white tone. This phenomenon was not observed in this case, indicating that the particles did not form. This result is in line with what was described by Alias et al.[33]. In their experiment, there was no formation of ZnO nanostructures in acidic and neutral mediums. These results seem to confirm that when the concentration of OH^- ions is lower, it becomes more difficult to form the growth unit $Zn(OH)_4^{2-}$ and consequently to obtain ZnO particles.

SG3 proceeded normally and the corresponding TEM images are shown in Figure 10, and the estimated values are shown in Table 3.

Table 3 - Results regarding the pH effect

Experiment	pH value	Average particle diameter (nm)	Average shape factor	Reaction Yield (%)
SG2	7	-	-	-
SG1	9	8 ± 1	1,2 ± 0,2	88
SG3	11	5 ± 1	1,1 ± 0,1	51

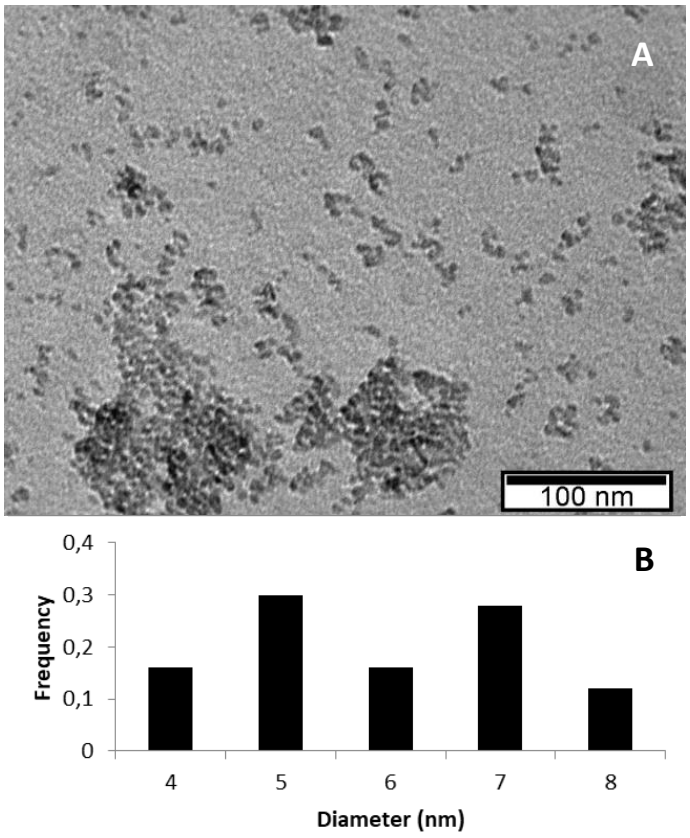

Figure 10 – A) TEM image of ZnO NPs synthesized at pH 11 and B) Diameter distribution of ZnO NPs synthesized at pH 11

The average diameter of the ZnO NPs obtained was 5 ± 1 nm, the average shape factor was 1,1 ± 0,1 and the reaction yield was 51%. Comparing this result with the control experiment (pH=9) it is possible to observe a decrease in yield and in the size of the nanoparticles with the increase of the pH value, in alkaline medium. This result is also in agreement with the literature [33][35]. In basic media, the formation of zinc oxide is favoured due to the decisive role of OH^- in the formation of the growth unit $Zn(OH)_4^{2-}$ (Equations 1 - 3). An increase in the pH value leads to an increase in nucleation and growth rates. This phenomenon affects the final size of the particles, as the results show, as more nuclei are formed. The same amount of material is distributed over more growing particles, resulting in smaller size nanoparticles. However, the reaction yield value significantly decreased from pH 9 to pH 11. This may be related to the dissolution effect of zinc oxide nanoparticles, mentioned by Alias et al.[33]. According to them, at higher pH values, dissolution of the particles was observed (Equation 3 – inverse reaction). This could be a possible explanation for the decrease in the reaction yield and, if so, this dissolution will also contribute to the decrease in the size of the final nanoparticles. In this way, the results show that, of the tested pH values, pH = 9 is the one that presents the best conditions, because it presents the highest yield and possibly is the value at which the particles are most stable. The shape of the particles does not change significantly with the change in pH value.

3.1.2 Influence of the precursor concentration

The initial precursor concentration was also varied to understand its effect on the final nanoparticles. Its value was changed to one third (*SG4*) and two thirds (*SG5*) of the control experiment, while the remaining conditions were kept constant (pH, solvent, reaction time and temperature). Figure 11 shows the TEM images for the *SG4* and *SG5* syntheses, as well as the corresponding diameter distribution analyses. The estimated size values are presented in Table 4.

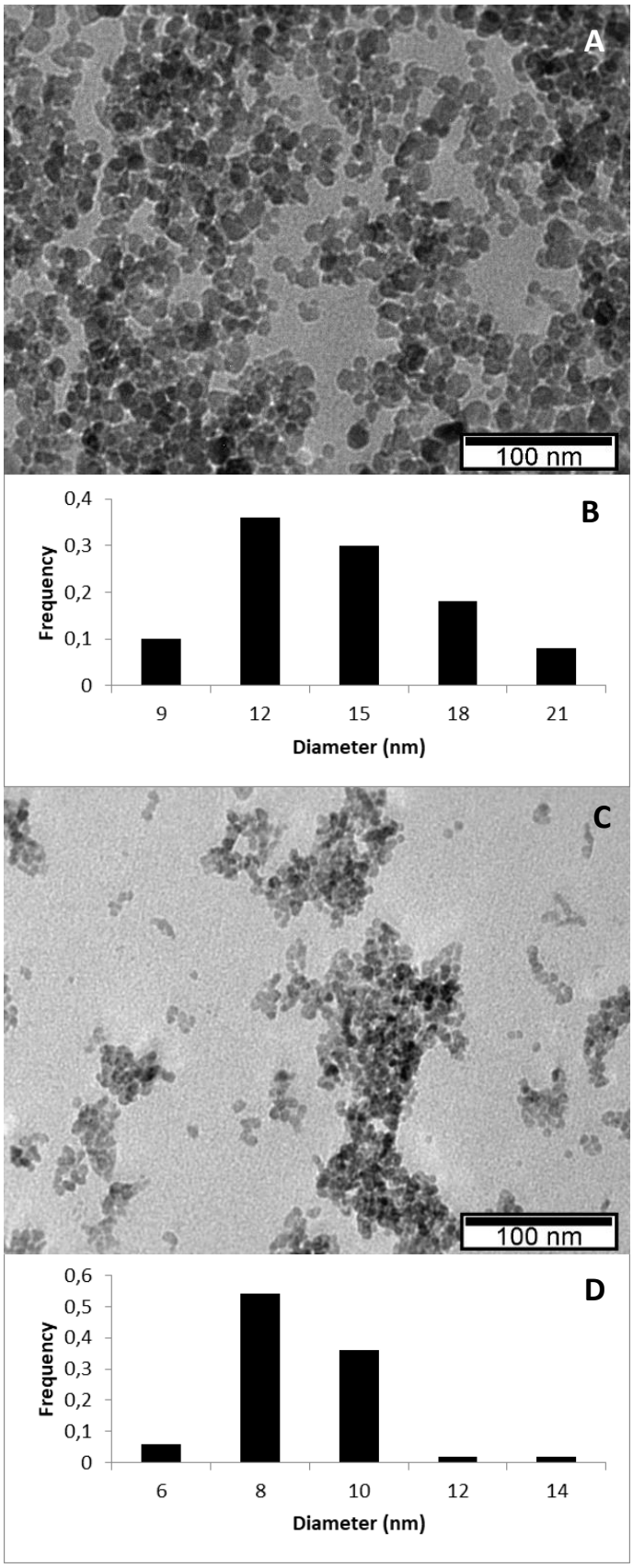

Figure 11 – TEM images (A and C) and diameter distribution (B and D) of ZnO NPs synthesized with a precursor concentration of 0.07M (A and B) and 0.13M (C and D).

Table 4 - Results regarding the precursor concentration effect

Experiment	Precursor concentration (M)	Average particle diameter (nm)	Average shape factor	Reaction Yield (%)
SG4	0.07	13 ± 3	1,2 ± 0,1	98
SG5	0.13	8 ± 1	1,2 ± 0,1	49
SG1	0.2	8 ± 1	1,2 ± 0,2	88

The average diameter of the ZnO NPs obtained was 13 ± 3 nm and 8 ± 1 nm for *SG4* and *SG5*, respectively, with average shape factors of 1,2 ± 0,1 and 1,2 ± 0,1. The corresponding reaction yield values are 98% and 49%.

According to Equation 8, the nucleation rate is expected to increase with increasing supersaturation, which is directly related with the precursor concentration. Fewer nuclei make bigger particles. Although the particle sizes did not vary from *SG1* to *SG5*, there was a clear increase in this parameter when observing *SG4* results. A broader interpretation of these results supports the expected growth behaviour, that particle size increases with decreasing concentration of the initial precursor. Despite the variation in particle sizes, the shape factor remained unchanged in the three experiments. Regarding the reaction yields, *SG4* approaches a value of 100%, while in *SG5* there was a decrease to approximately half of that value. Due to the high difference in these values and the lack of a clear pattern for evaluating them, no conclusion is drawn regarding this.

3.1.3 Influence of the synthesis solvent

The main objective of *SG6* was to test the use of a non-alcoholic solvent, more specifically water, and to understand its effect on the final nanoparticles. TEM images were taken (Figure 12), and the estimated values of the final diameter and shape factor are showed in Table 5. This synthesis was performed with one third of the precursor concentration of the control experiment, and as such, *SG4* is the experiment that serves as a comparison to *SG6* results, as they present the same amount of initial precursor.

Table 5 - Results regarding the solvent effect

Experiment	Solvent	Average particle diameter (nm)	Average shape factor	Reaction Yield (%)
SG4	Methanol	13 ± 3	1,2 ± 0,1	98
SG6	Water	370 ± 119	1,3 ± 0,2	85

The average diameter of the ZnO NPs obtained was 370 ± 119 nm, the average shape factor was 1,3 ± 0,2 nm and the reaction yield was 85%. An interpretation of these results must be made considering the values of dielectric constant and polarity of methanol and water, presented in Table 6.

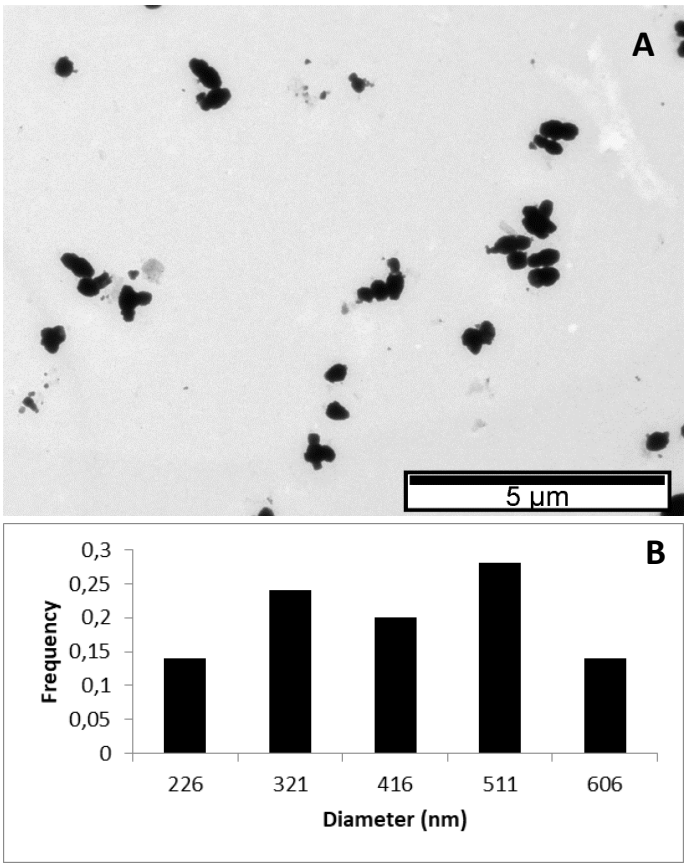

Figure 12 - A) TEM image of ZnO NPs synthesized by solvothermal method and B) Diameter distribution of ZnO NPs synthesized by solvothermal method

Table 6 - Solvent properties

Solvent	**Relative polarity** [59]	**Dielectric constant** [60]
Methanol	0,762	32
Water	1	80

A possible explanation for this large difference in the size results may be related to the electrostatic repulsive energy values. As previously mentioned, the electrostatic repulsive interaction energy is directly proportional to the polarity and inversely proportional to the dielectric constant of the solvent molecules (Equation 9). Among the two solvents, water possess the highest polarity, which in a first analysis would translate into an increase in repulsive interaction. However, at the same time, the dielectric constant of water appears to be large enough to reduce this repulsion, and to produce larger particles than the synthesis carried out in methanol. Regarding the reaction yields, *SG4* is not the best experiment for comparisons since there is no complete confidence in this result. However, the *ST* value is similar to that of *SG1* and is greater than 80%, so there are no large variations in the reaction yield that would allow one method to be preferred over another.

3.1.4 Influence of the reaction time

In *SG7* and *SG8*, the effect of the reaction time on the final nanoparticles was studied. Its value was changed from 0.5h (*SG7*) to 1h (*SG8*), while the remaining conditions were kept constant (pH, precursor concentration, solvent, and temperature). Figure 13 shows TEM images of the respective obtained nanoparticles. Table 7 presents the variations of the particle's diameter and shape factor for the considered syntheses.

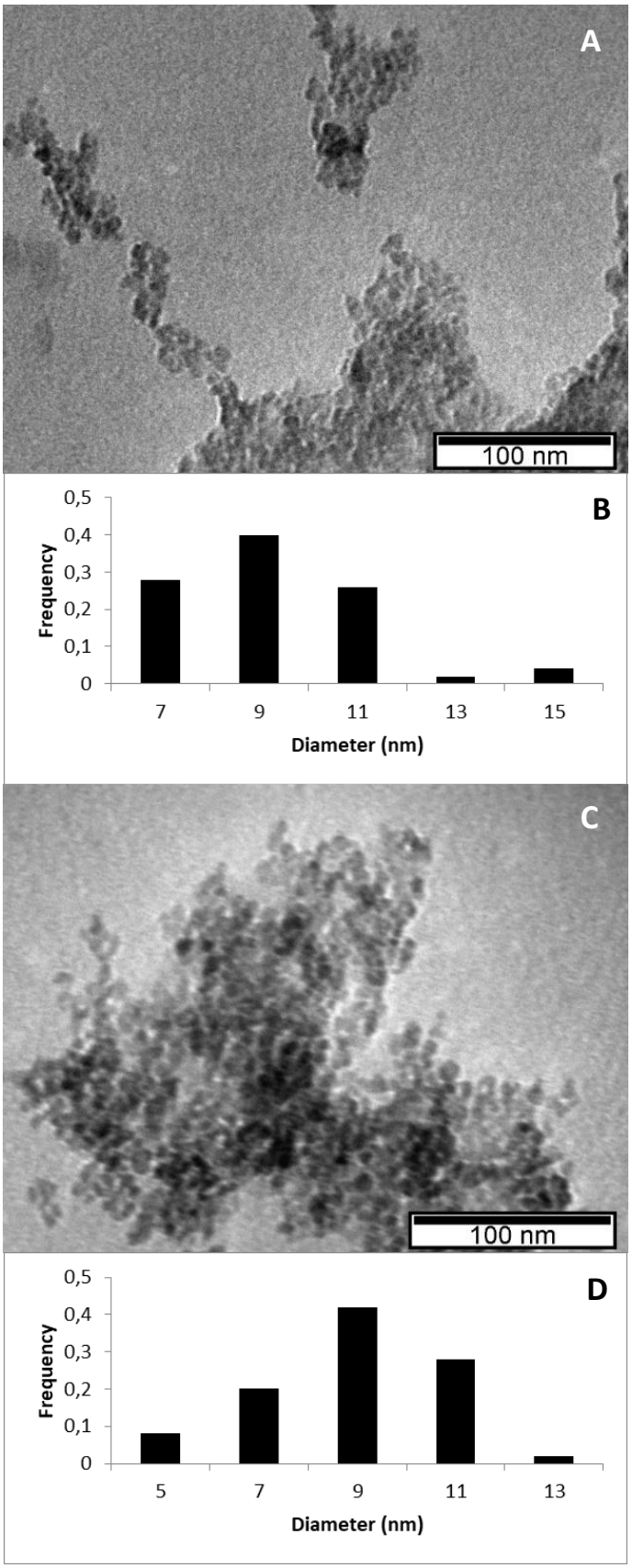

Figure 13 - TEM images (A and C) and diameter distribution (B and D) of ZnO NPs synthesized in 0.5h (A and B) and 1h (C and D)

Table 7 - Results regarding the influence of the reaction time

Experiment	Reaction time (h)	Average particle diameter (nm)	Average shape factor	Reaction Yield (%)
SG7	0.5	8 ± 2	1,2 ± 0,1	77
SG8	1	8 ± 2	1,1 ± 0,2	80
SG1	2.5	8 ± 1	1,2 ± 0,2	88

The average diameter of the obtained ZnO NPs was 8 ± 2 nm for both and average shape factors of 1,2 ± 0,1 and 1,1 ± 0,2 (*SG7* and *SG8*, respectively). The corresponding reaction yield values were 77% and 80%.

The results show that there was no change in the size of the nanoparticles and in the shape factor with the variation of the reaction time. This may indicate that in the first 0.5h of reaction, the particles are already formed and well established, so that the additional reaction time will not significantly affect the size of the nanoparticles. However, the reaction yield, which is an important factor to have into account, increased by 11% from 0.5h to 2.5h, suggesting that an increase in the reaction time will favour an increase in the reaction yield. This variation is significant and as such, for each case, a discussion should be made about which parameter is most valued, the time spent in the synthesis, or the amount of final product obtained.

According to Hu et al.[46], after nucleation and growth, the average particle size continues to increase with time due to coarsening mechanisms (Equation 10). In this case, this relationship was not verified, which may indicate that the coarsening mechanisms are not present, or that they would require much more time to be noticed.

3.1.5 Influence of the reaction temperature

In order to understand the effect of the reaction temperature on the final nanoparticles, its value was changed while the remaining conditions were kept constant (pH, precursor concentration, solvent and reaction time). Figure 14 shows TEM images of *SG9* (40ºC) and *SG10* (60ºC). Table 8 presents the variations of the particle's diameter and shape factor for the considered syntheses.

Table 8 - Results regarding the influence of the reaction temperature

Experiment	Reaction temperature (ºC)	Average particle diameter (nm)	Average shape factor	Reaction Yield (%)
SG1	Room Temp.	8 ± 1	1,2 ± 0,2	88
SG9	40	10 ± 2	1,3 ± 0,2	55
SG10	60	7 ± 2	1,2 ± 0,2	73

The average diameter of the obtained ZnO NPs was 10 ± 2 nm and 7 ± 2 nm for *SG9* and *SG10*, respectively, with average shape factors of 1,3 ± 0,2 and 1,2 ± 0,2. The corresponding reaction yield values were 55% and 73%.

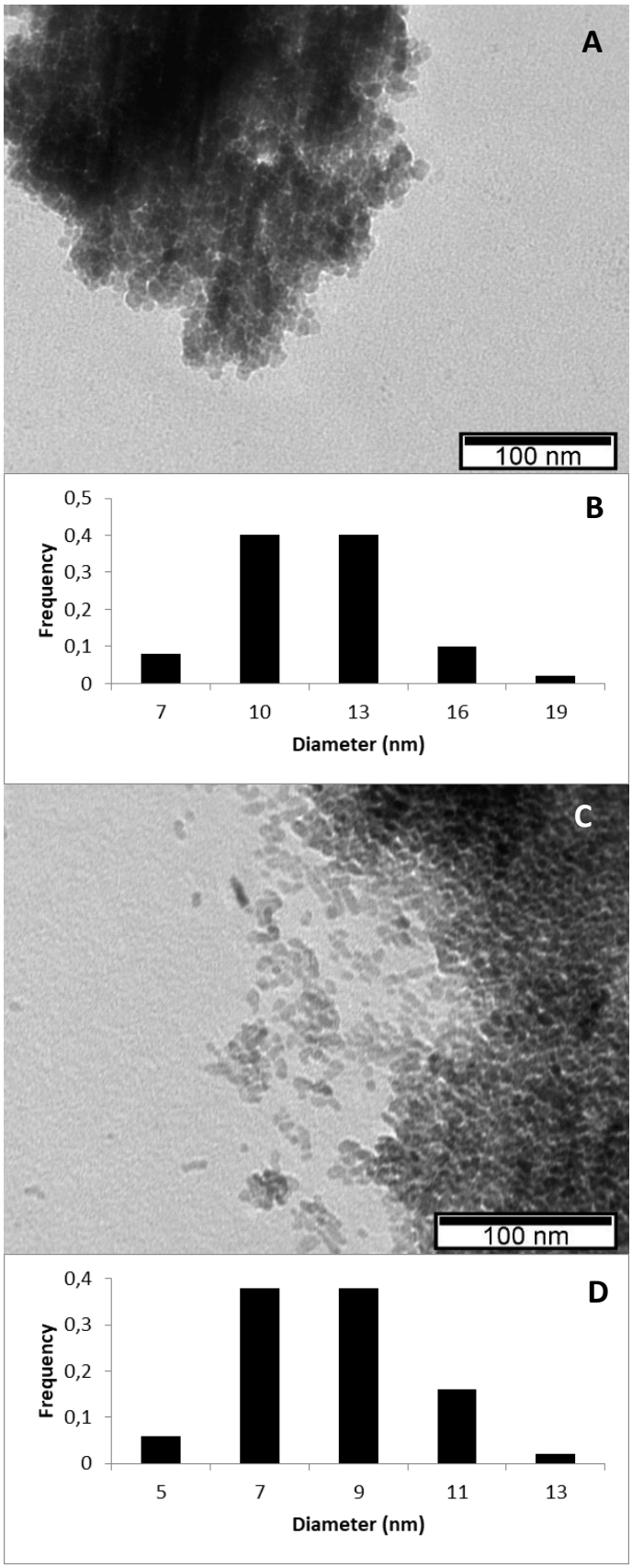

Figure 14 - TEM images (A and C) and diameter distribution (B and D) of ZnO NPs synthesized at 40˚C (A and B) and 60˚C (C and D).

Several synthesis parameters are temperature dependent. For higher temperatures, the nucleation rate decreases (Equation 8), which results in bigger final particles since the same amount of matter is distributed over less nuclei. Surface energy or solvent viscosity are other examples of factors that are influenced by temperature. The higher the temperature, the lower the surface energy and the lower the viscosity. Analysing the effect of these parameters on the coarsening rate constant (Equation 10), it is possible to notice that a decrease in surface energy contributes to decrease this constant, but a decrease in viscosity tends to increase it (here the temperature contributes simultaneously, but in different ways, to the increase and decrease of particle sizes by coarsening mechanisms). Since the reaction time results did not reveal the presence of coarsening mechanisms and changes in the particle size by these aging processes, it is possible that the aforementioned temperature effects also do not influence the size of the particles obtained.

The obtained results did not show a clear change in the particle size with the temperature variation and, as such, no conclusion should be drawn from this analysis. Regarding the particles morphology analysis, their shape is approximately spherical for the three experiments, with no alterations in the shape factor. Regarding the reaction yield values, the results were also not very clear. This parameter decreased 33% from room temperature to 40ºC and increased 18% from 40ºC to 60ºC. Once again, it was not verified a clear and logic variation and as such, no conclusions should be drawn from here.

3.2 Solvothermal synthesis and characterization of ZnO NPs

In order to compare the results obtained by sol-gel with other published methods to synthesize ZnO NPs, a solvothermal synthesis was performed, as described by Achouri et al. [56].The ZnO NPs were analysed by TEM imaging (Figure 15).

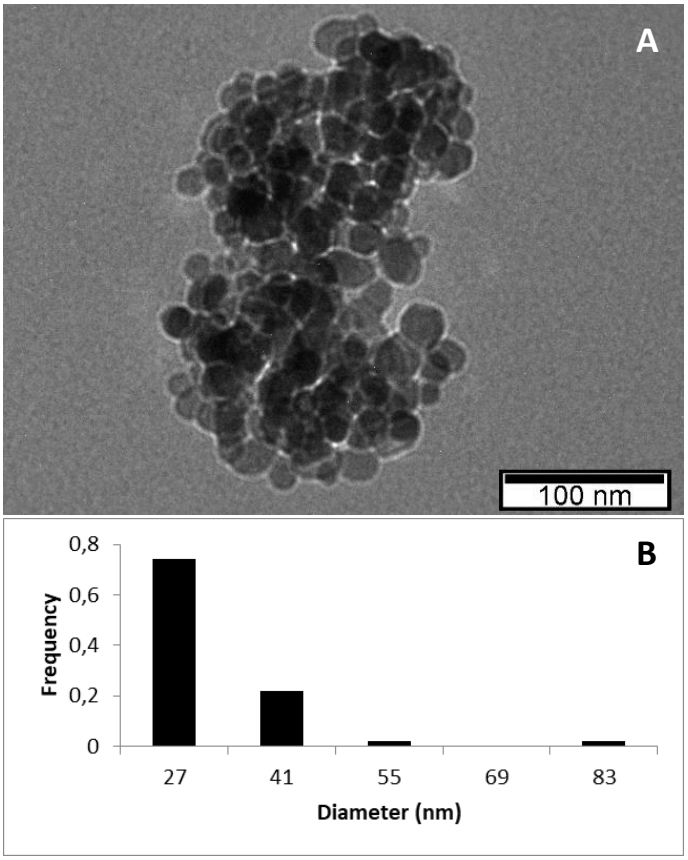

Figure 15 - A) TEM image of ZnO NPs synthesized by solvothermal method and B) Diameter distribution of ZnO NPs synthesized by solvothermal method

The obtained nanoparticles have an average particle diameter of 25 ± 11 nm and an average shape factor of 1,2 ± 0,1. The reaction yield was about 65%.

There are some differences in the synthesis parameters comparing the solvothermal experiment and the control experiment. Even so, the ones that have the greatest impact, as they present the greatest variation when compared, are the high temperature, high pressure and high reaction time. This reaction proceeded at 160°C for 24h in a Teflon-sealed autoclave.

The results show that the particle size obtained is larger than any of the previous (except the synthesis in water). Analysing the results, this solvothermal synthesis does not seem to bring morphological and size advantages when compared with the sol-gel syntheses. The increase in size may be an advantage or disadvantage, depending on the intended application, however the respective standard deviation is relatively high, the highest observed, indicating that the particles have more heterogeneous sizes. The morphology of the particles does not seem to have undergone great variation, presenting an approximately spherical shape. The reaction yield in this case is lower than most sol-gel experiments tested.

In the solvothermal method, by increasing temperature and pressure, the fundamental properties (e.g. viscosity, density, dielectric constant, etc) of the solvent change. As temperature increases, the dielectric constant decreases and the ionic species can precipitate, leading to the formation of the ZnO nanoparticles. However, the mechanisms controlling the reactions are more difficult to verify when compared with the sol-gel method.

Therefore, focusing only on the results obtained regarding the size and morphology of the nanoparticles, it does not seem that the solvothermal synthesis presents significant advantages over the sol-gel synthesis, unless one wants to obtain particles with larger sizes. Sol-gel is a simpler method than solvothermal, in which the evolution of particle growth can be more easily analyzed and can be carried out at room temperature.

3.3 ZnO mesoporous nanoparticles

One of the main objectives of this thesis was to test the possibility of producing mesoporous zinc oxide nanoparticles. For this purpose, two sol-gel syntheses were tested: *Meso1* and *Meso2*. Both correspond to adaptations of MSN syntheses however with the use of zinc precursors to obtain zinc oxide nanoparticles. *Meso1* was adapted from the experiment described by Ribeiro et al. [57] and *Meso2* from the synthesis performed by Rodrigues et al.[58]. *Meso1* was performed in water at 32ºC, with a NaOH solution as the base and *Meso2* was performed in water and ethanol, at 50ºC, with an ammonium hydroxide solution serving as the base. This was the starting point for trying to understand the mechanisms that could eventually originate this specific type of particles.

For both cases, the nanoparticles were analysed by TEM imaging (Figure 16 - *Meso1*, Figure 17 - *Meso2*).

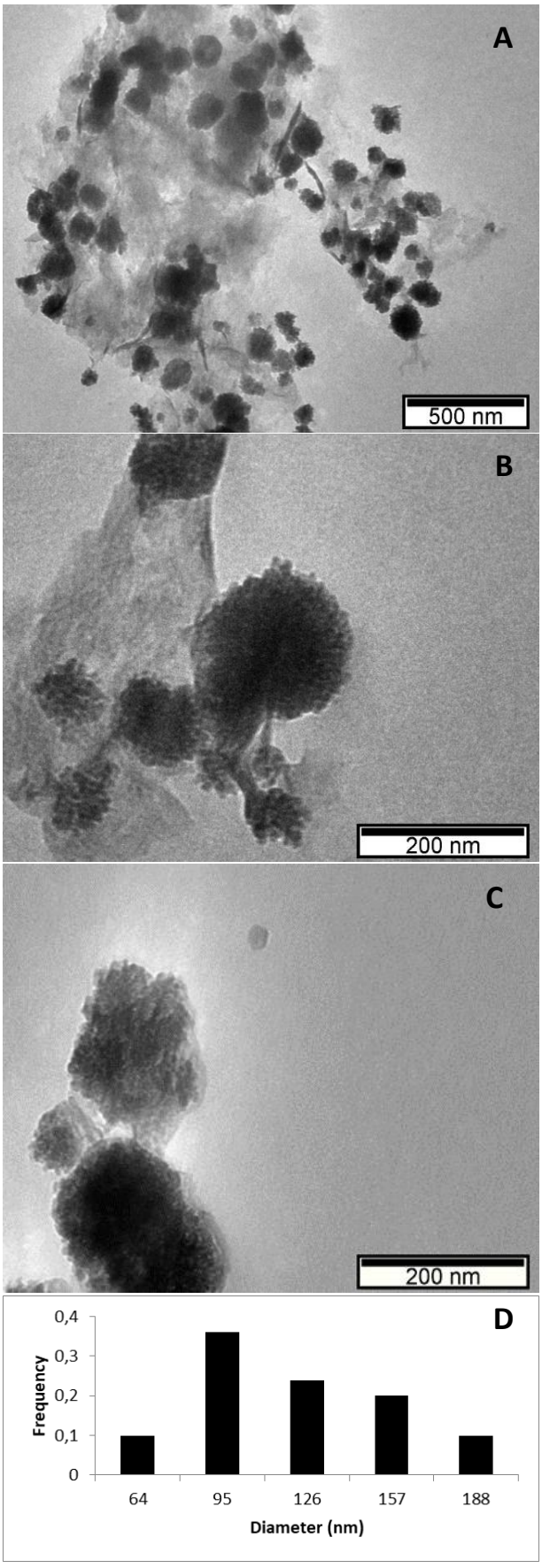

Figure 16 - A) TEM images of the MZNs obtained by the Meso1 synthesis (A, B and C) and diameter distribution (D)

The TEM images *Meso1* suggest the existence of mesoporous zinc oxide nanoparticles (MZNs) with an average diameter of 107± 39 nm, an average shape factor of 1.2 ± 0.1, and reaction yield of about 10%.

The formation of the expected mesoporous nanostructures, i.e. spherical nanoparticles with mesopores, is based on the use of a template, formed by the supramicellar assembly of cylindrical micelles. Once the zinc precursor is added, the hydrolysis/condensation reactions lead to the formation of zinc oxide around the micelles. The structural equilibrium of the supramicellar assembly is very susceptible to changes in the reaction system and if the ideal conditions are not obtained, the subsequent formation of these mesoporous particles is compromised. However, analyzing the obtained results, the growth of zinc oxide around micellar structures appears to have occurred.

Despite the relatively high standard deviation obtained, these results constitute a first base for the study of the formation of mesoporous zinc oxide nanostructures. More future studies will be necessary in order to verify the stability of these structures and to readjust the synthesis parameters to improve these results, especially the reaction yield which is very low.

The *Meso2* TEM images reveal structures composed of rod-shaped nanoparticles. Due to the difficulty in evaluating the individual dimensions and morphology of these nanoparticles, the corresponding measurements were not performed. However, it is possible to observe from the scale of the Figure 17 that these particles and aggregates are much larger than any other obtained within the scope of this thesis. The reaction yield was estimated to be around 23%, again a very low value.

These results are quite different from what was expected and from *Meso1*. It is not possible to compare the two syntheses since several synthesis parameters vary. The main conclusion that can be drawn from these results is that this synthesis is not suitable for producing mesoporous zinc oxide nanoparticles.

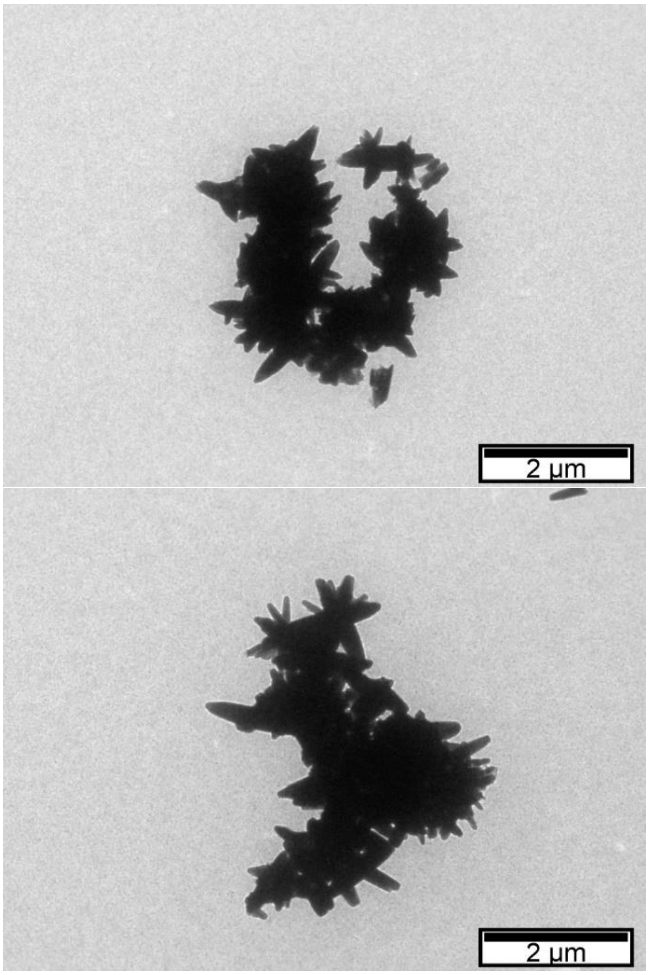

Figure 17 - TEM images of the structures obtained by Meso2

Chapter 4

Conclusions

With this work, we intended to understand the growth mechanism of zinc oxide nanoparticles by the sol-gel method in order to control their morphology. Initially, the influence of the synthesis parameters (pH, precursor concentration, solvent, reaction time and temperature) on the final zinc oxide nanoparticles was studied. Then a comparison of sol-gel synthesis with solvothermal synthesis was made. Finally, two attempts were made to produce mesoporous zinc oxide nanoparticles. The analysis of the results considered the diameters, morphology, and size distribution of the nanoparticles.

The syntheses carried out at different pH values (7, 9 and 11) allow us to conclude that in a basic medium, the formation of zinc oxide is favoured due to the higher concentration of OH^- ions, which play a fundamental role in the formation of the growth unit $Zn(OH)_4^{2-}$. In neutral medium, the concentration of these ions is lower, so there was an inability to form particles. In basic medium, it was found that the higher the pH value, the smaller the particle size. For higher pH values, the reaction yield value significantly decreases, possibly due to the dissolution of the nanoparticles. For the experiments tested, the pH value with the most promising results was pH=9. The analysis of the initial concentration of zinc precursor (0.07, 0.13 and 0.20 M) revealed that the size of the particles increases with decreasing precursor concentration. The experiments in which the solvent was studied (methanol and water) revealed that the synthesis carried out in water resulted in particles with diameters about 50 times larger than those in methanol, and with a much more heterogeneous size distribution. Some solvent properties, such as polarity or dielectric constant, seem to have a decisive role in the characteristics of the obtained nanoparticles. The reaction times analysed (0.5, 1 and 2.5 h) did not change the final nanoparticles, however an increase in the reaction time suggests an increase in the reaction yield. The temperature experiments (room temperature, 40ºC, 60ºC) were inconclusive since there was not a clear change behaviour of the particle size with the temperature variation. In all experiments, the nanoparticles showed an approximately spherical morphology.

The solvothermal synthesis performed did not present comparative advantages over the sol-gel method considering the parameters evaluated. Larger particles with a more heterogeneous size distribution were obtained and the reaction yield was lower for this method, when compared with sol-gel. The greater energy and time consumption of this synthesis and the lesser simplicity of the process compared to sol-gel justifies the use of the sol-gel method to produce ZnO NPs.

Of the mesoporous syntheses tested, the one that showed the most promising results was *Meso1*. It was possible to obtain mesoporous zinc oxide nanoparticles and, although the size distribution is broad, and the reaction yield is very low, it seems to be an excellent starting point for the future development and improvement of mesoporous zinc oxide nanoparticles.

Chapter 5

Future work

The inoperationality of the electronic microscopy equipment during most of this work, made it very difficult to optimize the different procedures earlier. With the present results, it would be necessary to evaluate the effect of the synthesis parameters on the optical properties of zinc oxide. The optical properties of zinc oxide are one of the main parameters that make this material so promising and interesting and as such should be studied. The discussion and conclusions of this thesis were based solely on the morphology and size of the nanoparticles. But it would be interesting to understand which synthesis conditions allow to obtain the most interesting optical properties.

A next step would be to try to understand and optimize the synthesis of mesoporous zinc oxide nanoparticles, combining the knowledge acquired in experiments that studied the influence of synthesis parameters. It would also be interesting to incorporate in the study of these nanoparticles other characterization techniques that allow a better understanding of the synthesis mechanisms, such as Brunauer-Emmett-Teller (BET) analysis, Uv-Vis spectroscopy or X-ray diffraction analysis.

Once synthesize stable mesoporous zinc oxide nanoparticles with interesting optical and morphological properties, it would be interesting to functionalize their surface and carry out loading and release tests of specific cargo molecules to understand their viability for drug delivery applications.

Bibliography

[1] Klingshirn, C., Hauschild, R., Priller, H., Decker, M., Zeller, J., & Kalt, H. ZnO rediscovered—once again!?. *Superlattices and Microstructures* **2005**, *38*(4-6), 209-222.

[2] Wibowo, A., Marsudi, M. A., Amal, M. I., Ananda, M. B., Stephanie, R., Ardy, H., & Diguna, L. J. ZnO nanostructured materials for emerging solar cell applications. *RSC advances* **2020**, *10*(70), 42838-42859.

[3] Djurišić, A. B., Ng, A. M. C., & Chen, X. Y. ZnO nanostructures for optoelectronics: Material properties and device applications. *Progress in quantum electronics* **2010**, *34*(4), 191-259.

[4] Mishra, P. K., Mishra, H., Ekielski, A., Talegaonkar, S., & Vaidya, B. Zinc oxide nanoparticles: a promising nanomaterial for biomedical applications. *Drug discovery today* **2017**, *22*(12), 1825-1834.

[5] Espitia, P. J. P., Soares, N. D. F. F., Coimbra, J. S. D. R., de Andrade, N. J., Cruz, R. S., & Medeiros, E. A. A. (2012). Zinc oxide nanoparticles: synthesis, antimicrobial activity and food packaging applications. *Food and bioprocess technology* **2012**, *5*(5), 1447-1464.

[6] Noman, M. T., Amor, N., & Petru, M. Synthesis and applications of ZnO nanostructures (ZONSs): A review. *Critical Reviews in Solid State and Materials Sciences* **2022**, *47*(2), 99-141.

[7] Uğur, Ş. S., Sarıışık, M., Aktaş, A. H., Uçar, M. Ç., & Erden, E. Modifying of cotton fabric surface with nano-ZnO multilayer films by layer-by-layer deposition method. *Nanoscale research letters* **2010**,*5*(7), 1204-1210.

[8] Klingshirn, C. ZnO: material, physics and applications. *ChemPhysChem* **2007**, *8*(6), 782-803.

[9] Chen, H., Li, C., Zhang, X., & Yang, W. ZnO nanoplates with abundant porosity for significant formaldehyde-sensing. *Materials Letters* **2020**, *260*, 126982.

[10] Song, Y., Chen, F., Zhang, Y., Zhang, S., Liu, F., Sun, P., ... & Lu, G. Fabrication of highly sensitive and selective room-temperature nitrogen dioxide sensors based on the ZnO nanoflowers. *Sensors and Actuators B: Chemical* **2019**, *287*, 191-198.

[11] Kang, Y., Yu, F., Zhang, L., Wang, W., Chen, L., & Li, Y. Review of ZnO-based nanomaterials in gas sensors. *Solid State Ionics* **2021**, *360*, 115544.

[12] Ong, C. B., Ng, L. Y., & Mohammad, A. W. A review of ZnO nanoparticles as solar photocatalysts: Synthesis, mechanisms and applications. *Renewable and Sustainable Energy Reviews* **2018**, *81*, 536-551.

[13] Sabir, S., Arshad, M., & Chaudhari, S. K. Zinc oxide nanoparticles for revolutionizing agriculture: synthesis and applications. *The Scientific World Journal*, **2014**

[14] Nguyen, T. D., & Do, T. O. Size-and shape-controlled synthesis of monodisperse metal oxide and mixed oxide nanocrystals. *Nanocrystal* **2011**, *66*, 55-84.

[15] Khan, I., Saeed, K., & Khan, I. Nanoparticles: Properties, applications and toxicities. *Arabian journal of chemistry* **2019**, *12*(7), 908-931.

[16] Wirunchit, S., Gansa, P., & Koetniyom, W. Synthesis of ZnO nanoparticles by Ball-milling process for biological applications. *Materials Today: Proceedings* **2021**, *47*, 3554-3559.

[17] Papageorgiou, G. P., Karydas, A. G., Papageorgiou, G., Kantarelou, V., & Makarona, E. Controlled synthesis of periodic arrays of ZnO nanostructures combining e-beam lithography and solution-based processes leveraged by micro X-ray fluorescence spectroscopy. *Micro and Nano Engineering* **2020**, *8*, 100063.

[18] Chaker, A., Alty, H. R., Tian, P., Kotsovinos, A., Timco, G. A., Muryn, C. A., ... & Winpenny, R. E. Nanoscale patterning of zinc oxide from zinc acetate using electron beam lithography for the preparation of hard lithographic masks. *ACS Applied Nano Materials* **2020**, *4*(1), 406-413.

[19] Ismail, A. M., Menazea, A. A., Kabary, H. A., El-Sherbiny, A. E., & Samy, A. The influence of calcination temperature on structural and antimicrobial characteristics of zinc oxide nanoparticles synthesized by Sol–Gel method. *Journal of Molecular Structure* **2019**, *1196*, 332-337.

[20] Ba-Abbad, M. M., Takriff, M. S., Benamor, A., Nasser, M. S., Mahmoudi, E., & Mohammad, A. W. Synthesis and characterization of Sm3+-doped ZnO nanoparticles via a sol–gel method and their photocatalytic application. *Journal of Sol-Gel Science and Technology* **2018**, *85*(1), 178-190.

[21] Wasly, H. S., Abd El-Sadek, M. S., & Henini, M. Influence of reaction time and synthesis temperature on the physical properties of ZnO nanoparticles synthesized by the hydrothermal method. *Applied Physics A*, **2018**, *124*(1), 1-12.
[22] Agarwal, S., Rai, P., Gatell, E. N., Llobet, E., Güell, F., Kumar, M., & Awasthi, K. Gas sensing properties of ZnO nanostructures (flowers/rods) synthesized by hydrothermal method. *Sensors and Actuators B: Chemical* **2019**, *292*, 24-31.
[23] Adam, R. E., Pozina, G., Willander, M., & Nur, O. Synthesis of ZnO nanoparticles by co-precipitation method for solar driven photodegradation of Congo red dye at different pH. *Photonics and Nanostructures-Fundamentals and Applications* **2018**, *32*, 11-18.
[24] Katiyar, A., Kumar, N., Shukla, R. K., & Srivastava, A. Influence of alkali hydroxides on synthesis, physico-chemical and photoluminescence properties of zinc oxide nanoparticles. *Materials Today: Proceedings* **2020**, *29*, 885-889.
[25] Agarwal, H., Kumar, S. V., & Rajeshkumar, S. A review on green synthesis of zinc oxide nanoparticles–An eco-friendly approach. *Resource-Efficient Technologies* **2017**, *3*(4), 406-413.
[26] Singh, T. A., Das, J., & Sil, P. C. Zinc oxide nanoparticles: A comprehensive review on its synthesis, anticancer and drug delivery applications as well as health risks. *Advances in Colloid and Interface Science* **2020**, *286*, 102317.
[27] Parashar, M., Shukla, V. K., & Singh, R. Metal oxides nanoparticles via sol–gel method: a review on synthesis, characterization and applications. *Journal of Materials Science: Materials in Electronics* **2020**, *31*(5), 3729-3749.
[28] Ensafi, A. A., Saberi, Z., & Kazemifard, N. Functionalized nanomaterial-based medical sensors for point-of-care applications: An overview. *Functionalized Nanomaterial-Based Electrochemical Sensors* **2022**, 277-308.
[29] Yilmaz, E., & Soylak, M. Functionalized nanomaterials for sample preparation methods. In *Handbook of Nanomaterials in analytical chemistry* **2020** ,375-413
[30] Sridevi, K. P., Sivakumar, S., & Saravanan, K. Synthesis and Characterizations of Zinc Oxide Nanoparticles Using Various Precursors. *Annals of the Romanian Society for Cell Biology* **2021**, 8679-8689.
[31] Thein, M. T., Pung, S. Y., Aziz, A., & Itoh, M. The role of ammonia hydroxide in the formation of ZnO hexagonal nanodisks using sol–gel technique and their photocatalytic study. *Journal of Experimental Nanoscience* **2015**, *10*(14), 1068-1081.
[32] Gyawali, S., Goni, L. K. M. O., Chowdhury, M. S., Laref, A., Bajgai, S., Chantrapromma, S., & Techato, K. Effect of KOH concentration on the properties of ZnO nanoparticles. *Materials Research Express* **2022**, *9*(5), 055004.
[33] Alias, S. S., Ismail, A. B., & Mohamad, A. A. Effect of pH on ZnO nanoparticle properties synthesized by sol–gel centrifugation. *Journal of Alloys and Compounds* **2010**, *499*(2), 231-237.
[34] Mahdavi, R., & Talesh, S. S. A. The effect of ultrasonic irradiation on the structure, morphology and photocatalytic performance of ZnO nanoparticles by sol-gel method. *Ultrasonics Sonochemistry* **2017**, *39*, 504-510.
[35] Li, W. J., Shi, E. W., & Fukuda, T. Particle size of powders under hydrothermal conditions. *Crystal Research and Technology: Journal of Experimental and Industrial Crystallography* **2003**, *38*(10), 847-858.
[36] Thanh, N. T., Maclean, N., & Mahiddine, S. Mechanisms of nucleation and growth of nanoparticles in solution. *Chemical reviews* **2014**, *114*(15), 7610-7630.
[37] Viswanatha, R., & Sarma, D. D. Growth of Nanocrystals in Solution. *Nanomaterials Chemistry: Recent Development and New Directions* **2007**, 139–170.
[38] La Mer, V.K., Dinegar, R.H., Theory, Production and Mechanism of Formation of Monodispersed Hydrosols, *J. Am. Chem. Soc* **1950**, *72*, 4847.
[39] Oskam, G. Metal oxide nanoparticles: synthesis, characterization and application. *Journal of sol-gel science and technology* **2006**, *37*(3), 161-164.
[40] Agrawal, D. C. *Introduction to nanoscience and nanomaterials* **2013**, World Scientific Publishing Company.
[41] Santos, L. S. L. *Engineering of Metal Oxide Nanoparticles for Application in Electrochemical Devices* **2015**, Universidade NOVA de Lisboa (Portugal).
[42] Wahab, R., Ansari, S. G., Kim, Y. S., Song, M., & Shin, H. S. The role of pH variation on the growth of zinc oxide nanostructures. *Applied Surface Science* **2009**, *255*(9), 4891-4896.

[43] Oskam, G., & Poot, F. D. J. P. Synthesis of ZnO and TiO2 nanoparticles. *Journal of sol-gel science and technology* **2006**, *37*(3), 157-160.
[44] De Yoreo, J. J., & Vekilov, P. G. Principles of crystal nucleation and growth. *Reviews in mineralogy and geochemistry* **2003**, *54*(1), 57-93.
[45] Ramya, M., Nideep, T. K., Nampoori, V. P. N., & Kailasnath, M. Solvent assisted evolution and growth mechanism of zero to three dimensional ZnO nanostructures for dye sensitized solar cell applications. *Scientific reports* **2021**, *11*(1), 1-14.
[46] Hu, Z., Oskam, G., & Searson, P. C. Influence of solvent on the growth of ZnO nanoparticles. *Journal of colloid and interface science* **2003**, *263*(2), 454-460.
[47] Ramya, M., Nideep, T. K., Nampoori, V. P. N., & Kailasnath, M. Understanding the role of alcohols in the growth behaviour of ZnO nanostructures prepared by solution based synthesis and their application in solar cells. *New Journal of Chemistry* **2019**, *43*(46), 17980-17990.
[48] McNaught, A. D., & Wilkinson, A. Compendium of chemical terminology **1997**, IUPAC recommendations.
[49] Barick, K. C., Nigam, S., & Bahadur, D. Nanoscale assembly of mesoporous ZnO: A potential drug carrier, *Journal of Materials Chemistry* **2010**, *20*(31), 6446-6452.
[50] Wu, S. H., Mou, C. Y., & Lin, H. P. Synthesis of mesoporous silica nanoparticles. Chemical Society Reviews **2013**, 42(9), 3862-3875.
[51] Baleizão, C., & Farinha, J. P. S. Hybrid smart mesoporous silica nanoparticles for theranostics. *Nanomedicine*, **2015**, *10*(15), 2311-2314.
[52] Gonçalves, J. L. M., Baleizão, C., & Farinha, J. P. S. Smart Porous Silica–Polymer Nanomaterials for Theranostics. *Soft Matter for Biomedical Applications* **2021**, *13*, 365.
[53] Lu, X., Zhang, H., Ni, Y., Zhang, Q., & Chen, J. Porous nanosheet-based ZnO microspheres for the construction of direct electrochemical biosensors. *Biosensors and bioelectronics* **2008**, *24*(1), 93-98.
[54] Bakrudeen, H. B., Sugunalakshmi, M., & Reddy, B. S. Auto-fluorescent mesoporous ZnO nanospheres for drug delivery carrier application. *Materials Science and Engineering: C* **2015**, *56*, 335-340.
[55] Rosa, P. A. S. *Glutathione-Responsive Breakable Nanoparticles for Controlled Doxorubicin Release*, [Master's Thesis, Instituto Superior Técnico], **2021**.
[56] Achouri, F., Corbel, S., Balan, L., Mozet, K., Girot, E., Medjahdi, G., & Schneider, R. Porous Mn-doped ZnO nanoparticles for enhanced solar and visible light photocatalysis. *Materials & Design* **2016**, *101*, 309-316.
[57] Ribeiro, T., Rodrigues, A. S., Calderon, S., Fidalgo, A., Gonçalves, J. L., André, V., Duarte, M.T., Ferreira, P.J., Farinha, J. P. S., Baleizão, C. Silica nanocarriers with user-defined precise diameters by controlled template self-assembly. *Journal of colloid and interface science* **2020**, *561*, 609-619.
[58] Rodrigues, A. S., Ribeiro, T., Fernandes, F., Farinha, J. P. S., & Baleizão, C. Intrinsically fluorescent silica nanocontainers: A promising theranostic platform. *Microscopy and Microanalysis* **2013**, *19*(5), 1216-1221.
[59] Welton, T., & Reichardt, C. *Solvents and solvent effects in organic chemistry*. (4th ed) John Wiley & Sons, **2011**, 455-461.
[60] Akerlof, G. Dielectric constants of some organic solvent-water mixtures at various temperatures. *Journal of the American Chemical Society* **1932**, *54*(11), 4125-4139.